HHS Public Access

Author manuscript

FEBS Lett. Author manuscript; available in PMC 2019 November 01.

Published in final edited form as:

FEBS Lett. 2018 November ; 592(21): 3563–3585. doi:10.1002/1873-3468.13270.

Toward a unified picture of the exocytotic fusion pore

Erdem Karatekin[1,2,3,4]

[1]Department of Cellular and Molecular Physiology, Yale University, New Haven, CT, USA

[2]Department of Molecular Biophysics and Biochemistry, Yale University, New Haven, CT, USA

[3]Nanobiology Institute, Yale University, West Haven, CT, USA

[4]Centre National de la Recherche Scientifique (CNRS), Paris, France

Abstract

Neurotransmitter and hormone release involve calcium-triggered fusion of a cargo-loaded vesicle with the plasma membrane. The initial connection between the fusing membranes, called the fusion pore, can evolve in various ways, including rapid dilation to allow full cargo release, slow expansion, repeated opening-closing, and resealing. Pore dynamics determine the kinetics of cargo release and the mode of vesicle recycling, but how these processes are controlled are poorly understood. Previous reconstitutions could not monitor single pores, limiting mechanistic insight they could provide. Recently developed nanodisc-based fusion assays allow reconstitution and monitoring of single pores with unprecedented detail and hold great promise for future discoveries. They recapitulate various aspects of exocytotic fusion pores, but comparison is difficult because different approaches suggested very different exocytotic fusion pore properties, even for the same cell type. In this Review, I discuss how most of the data can be reconciled, by recognizing how different methods probe different aspects of the same fusion process. The resulting picture is that fusion pores have broadly distributed properties arising from stochastic processes which can be modulated by physical constraints imposed by proteins, lipids and membranes.

1. INTRODUCTION

Calcium-triggered exocytosis is the basis of neurotransmitter release from neurons and hormone release from neuroendocrine cells [1–5]. Cytosolic calcium concentration is low, below ~100 nM. A ~10^4 times larger extracellular calcium concentration provides a strong electrochemical driving force for calcium entry into the cell when the cell membrane is depolarized, causing voltage-gated calcium channels to open. In a hormone secreting cell, secretory granules (~150–300 nm diameter) laden with a mixture of small molecules such as catecholamines and larger peptides fuse with the plasma membrane upon an increase in intracellular calcium that follows depolarization. In neurons, a similar process occurs during neurotransmitter release, but the synaptic vesicles that fuse with the plasma membrane are much smaller (~40 nm diameter [6]) and they do not contain large, electron-dense cargo.

Key molecular components that act at late stages of exocytosis have been identified and are remarkably similar both for hormone and neurotransmitter release [3,7] (Figure 1). Once a vesicle is delivered to a release site, it undergoes “priming” to become fusion-ready. A

number of proteins have been implicated in priming and a clear mechanism is emerging for some, including Munc18 and Munc13 [5,8,9]. SNARE proteins are both necessary [10] and sufficient [11] for membrane fusion, and constitute the core of the fusion machinery [1]. Assembly of vesicular v- and target t-SNARE proteins into a coiled coil drives fusion [12,13]. Fusion is prevented under resting, low calcium levels by the synergistic action of Synaptotagmin-1 and Complexin [9,14]. When calcium near a release site increases, it binds Synaptotagmin's C2 domains and triggers fusion [15]. Calcium-binding to Synaptotagmin causes hydrophobic residues at the tips of the calcium-binding loops to insert into the bilayer, generating curvature, which may be coupled to fusion triggering [16–18].

The initial connection between the vesicle and the plasma membrane during exocytosis is called the "fusion pore" which is a key intermediate during the fusion reaction [19–23]. The fusion pore can flicker open-closed multiple times before resealing or dilating further. Pore dynamics determine the kinetics and extent of cargo release, and the mode of vesicle recycling. Fusion pores that re-seal after transient fusion lead to recapture of nearly-intact vesicles, whereas vesicles that fully fuse with the plasma membrane need to be regenerated *de novo* to maintain steady state vesicle densities. Thus, pore dynamics affect coupling of exo- and endocytosis, and vesicle recycling rates [24,25]. Slow release of neurotransmitter through small, flickering pores may deactivate post-synaptic receptors [26,27] and regulate the spatial extent of dopamine signaling [28]. In neuroendocrine cells where cargo of various sizes are co-packaged, pore dynamics also determine the nature of the cargo released: small fusion pores only allow release of sufficiently small cargo such as ATP [29,30] or catecholamines [31] and retain larger ones [29–31]. Reduced glucose-induced insulin release in type 2 diabetes has recently been linked to non-dilating small fusion pores that are too small to allow the exit of insulin [29].

Despite their importance, mechanisms controlling pore dynamics are poorly understood. Recent experiments, both in hormone-secreting neuroendocrine cells [29,32–34] and novel, nanodisc-based biochemical reconstitutions [35–41] have provided new insights into fusion pore dynamics. Here I will review nanodisc-based fusion assays and compare them with measurements of fusion pores in neuroendocrine cells. Fusion pore properties measured by different cell-based and reconstitution approaches are consistent with a picture in which the pores have broad lifetime and size distributions, lasting from a fraction of a second to ~100 s, and reaching sizes near vesicular diameters that can nevertheless revert to smaller sizes and eventually reseal.

2. NANODISC-BASED FUSION ASSAYS: A NEW LOOK AT FUSION PORES

Lipid bilayers do not like having edges exposed to aqueous solvent [42–44], hence tend to form closed structures such as vesicles and tubes. It is possible to obtain stable, flat bilayer structures only if the hydrophobic edges can be stabilized by "edge-acting" compounds [44] such as proteins [45–49], synthetic polymers [50], or short-chain lipids [51]. When the belt stabilizing the edges of the flat phospholipid disc is an engineered Apolipoprotein A1derivative called membrane scaffold protein (MSP), the resulting structure is called a nanodisc (ND, Figure 2A) [46,47], although the term has been used loosely to describe any stabilized flat, phospholipid bilayer of ~10–20 nm diameter. Other apolipoprotein derivatives

such as apoE422K [48,52] and covalent circularization [49] have been used to obtain larger discs, up to 30–50 nm in diameter (Figure 2A). Chromy et al. [48] refer to flat phospholipid assemblies whose edges are stabilized by any apolipoprotein derivative as nanolipoprotein particles (NLPs). I will use NLP and ND interchangeably, and specify the composition of the stabilizing belt when necessary.

NDs have traditionally been used in structural studies of membrane proteins and/or membrane-protein interactions (Fig. 2) [46]; their first application to studies of membrane fusion is much more recent [36]. The interest in using NDs in fusion studies arises from the following properties. First, the initially flat bilayer structure of a ND results in a pore that connects the compartment enclosed by the target membrane to the exterior space after fusion. By contrast, when two closed bilayer structures such as two liposomes fuse, the result is again a closed structure, another liposome. It is difficult to directly probe the fusion pore during such a fusion reaction [53]. Second, copy numbers of proteins reconstituted into a ND can be controlled tightly [35–37,41]. Third, using different scaffold proteins and lipid-to-scaffold protein ratios, one can vary disc size. Small discs (diameter $\lesssim$ 15 nm) prevent expansion of the pore beyond a few nm in diameter and thus permit isolation of the initial stages of the small fusion pore [36,38,40]. Using large discs ($\gtrsim$ 20 nm) one can probe later stages of pore dilation, since the maximum pore size imposed by the scaffold will be larger (e.g. maximum pore diameter $\gtrsim$ 10 nm in refs. [35,37]). To be useful for membrane fusion studies, a nanodisc needs to be stable, i.e. there should be no spontaneous lipid exchange between discs. This condition is met by NLPs [35–38].

New venues afforded using NDs in membrane fusion studies will become evident below, when I review a few novel fusion assays involving NDs. Many more approaches are possible and are actively being explored.

2.1 Nanodisc-liposome fusion

The first use of nanodiscs in membrane fusion studies was pioneered by Shi et al. [36] who used ~15 nm diameter MSP NDs. They reconstituted increasing copy numbers of the neuronal v-SNARE VAMP2 (also known as Synaptobrevin-2, Syb2) into NDs and used them as fusion partners with small liposomes filled with ~50 mM $Ca^{2+}$and bearing cognate neuronal t-SNAREs composed of Syntaxin-1 and SNAP25. In parallel experiments, lipid mixing was assessed using a fluorescence dequenching approach [11]. Release of Ca^{2+} due to ND-liposome fusion was detected using a Ca^{2+} sensitive dye, present in the reaction medium (Fig. 2B). Shi et al. found that efficient lipid mixing occurred even with ~1 v-SNARE per disc, but calcium release required at least ~3 copies of the neuronal v-SNARE per disc face. This suggested a very small and/or transient pore could be induced by a single SNARE complex (which is sufficient to maintain two bilayers in close proximity [54]), but a larger/longer-lived pore that allowed detectable calcium release required three or more complexes [36]. Bello et al. [35] extended these studies by systematically varying both the size of cargo encapsulated into t-SNARE liposomes and v-SNARE copy numbers in larger, ~23 nm NLPs. There was a positive correlation between v-SNARE copies per disc and the size of cargo that could be released efficiently [35].

Using very small, ~6 nm diameter discs, Bao et al. [40] tested the idea that the initial fusion pore may be a channel-like structure whose walls are composed of the transmembrane domains (TMDs) of the neuronal SNAREs [19,21,55]. The rationale was that with such small discs fusing with liposomes, there was not enough space for a toroidal, lipid-lined pore to form; hence any detectable cargo release should occur through a different type of pore. Glutamate was encapsulated into the t-SNARE liposomes and the fluorescent glutamate sensor iGluSnFR was present in the bath to monitor release through fusion pores. Two copies of v-SNARE per ND face were sufficient for both efficient lipid mixing and cargo release. The results did not unequivocally support a lipid-lined or channel-like structure, in part because a maximum of only ~2 copies/face of the v-SNARE could be reconstituted into 6 nm discs, whereas formation of a channel-like structure large enough to release glutamate would require more [21,55]. Nevertheless, it was found that certain TMD residues were exposed to aqueous solution during fusion, which led the authors to propose that the fusion pores in the assay were composed both of lipid and TMDs [40].

In a later study, Bao et al. tethered single, t-SNARE reconstituted small liposomes filled with a soluble fluorescent dye, sulforhodamine B, onto a coverslip and monitored release of the dye upon fusion with v-SNARE reconstituted, ~13 nm diameter MSP NDs using total internal reflection fluorescence microscopy (TIRFM) [41]. Typical release time was ~1 s for NDs bearing 3–4 v-SNAREs per face, suggesting the fusion pore hindered release considerably, since the small probe ($D \approx 1\ \mu m^2/ms$) would only take ~10 μs to explore the lumen of a 100 nm liposome.

These ND-liposome studies are much easier to conduct than the single-pore measurements described below but could not directly provide information about fusion pore lifetimes or sizes.

2.2 Nanodisc-cell fusion

We fused v-SNARE reconstituted ~15 nm diameter MSP NDs with engineered cells expressing the complementary t-SNAREs ectopically in a “flipped” configuration [38] (Fig. 2C). The flipped t-SNARE cells were developed by the Rothman lab for cell-cell fusion studies with complementary flipped v-SNARE cells [14,56,57]. Fusion of a ND with the flipped t-SNARE cell membrane opens a small pore that connects the cell’s cytosol to the exterior of the cell, like an ion channel in the plasma membrane. This configuration allows use of ion-channel methods to probe ND-cell fusion pores (Fig. 2C).

Before attempting to measure single fusion pore conductances, we used a simple experiment to test whether fusion was specifically driven by SNAREs (Fig. 2C, top). We loaded flipped t-SNARE cells with a calcium sensitive fluorophore, Fluo-4, before adding v-SNARE NDs to the medium [38]. Upon fusion between discs and a flipped t-SNARE cell, a fusion pore opens and allows calcium influx into the cytosol, reported by an increase in Fluo-4 fluorescence. Control experiments with wild-type cells that do not express flipped t-SNAREs, using empty discs, or discs loaded with a mutant v-SNARE (VAMP2–4×, carrying mutations in the C-terminal hydrophobic layers, L70D, A74R, A81D, and L84D) that can dock membranes but cannot induce their fusion [58,59], did not result in calcium influx [38]. Thus, vNDs fuse with flipped t-SNARE cells in a SNARE-dependent manner.

Single fusion pores were detected [37,38] by use of cell-attached, voltage-clamp measurements, commonly employed to detect single ion-channel currents [60,61]. A small patch on a flipped t-SNARE cell is electrically isolated by tightly adhering a glass pipette onto the cell. The pipette solution is filled with a disc-free solution at the tip, and back-filled with v-SNARE nanodiscs. This allows tight seal formation and recording of a stable baseline before the nanodiscs diffuse to the pipette tip and fusion starts [38]. Fusion results in current bursts that typically return to baseline transiently and last several seconds before conductance is lost (Fig. 2C, bottom, and Fig. 3A). The rate at which such bursts appear increases with time, since the disc concentration near the cell surface increases [38]. This results in increasingly smaller number of currents that are well separated from one another. Because such pores are excluded from analysis, fusion rates are underestimated in this assay, especially in cases where the fusion rate is high. Whole-cell recordings are also possible, as depicted in Figure 2C, middle.

Detection of single pores relies on having a slow fusion rate: current bursts that appear infrequently are most likely to be due to single pores. A consistency check is provided by the maximum pore size allowed by the scaffold ring. For ~15 nm MSP discs, simple geometric arguments suggest pores should be limited to $\lesssim$ 4 nm diameter [36]. Indeed maximum pore sizes estimated from conductance distributions were limited to these values [38]. Note that pore size estimation from conductance measurements is approximate, since details of pore geometry are not known. Most of the literature assumes a 15 nm long cylindrical pore to estimate the pore radius [19] and we follow this convention. I tried to report both reported conductance values and the pore size corresponding to a 15 nm long cylinder throughout.

Unlike single ion-channel currents, most fusion pore currents fluctuate strongly and do not have well-defined, stable conductance levels (Fig. 2C, bottom, and Fig. 3A). To prevent exclusion of low conductance signals from analysis, we set a threshold close to the baseline and a minimum threshold-crossing duration to detect open sub-periods in a burst [38,62]. Pore properties exhibit broad distributions (Fig. 3). Pore lifetimes and number of flickers (open sub-periods during a burst) are well-described by an exponential and geometric function, respectively, with pores typically flickering ~10 times and lasting ~5–15 s, with some increase in these values with increasing pore size [37,38]. Single-pore conductance values are also broadly distributed, with the most likely conductance corresponding to a ~1 nm diameter pore, independent of SNARE copies per disc, or disc size [37,38]. This is much smaller than the maximum limits imposed by ND size, which are only reached by transient fluctuations [37,38].

Using fusion of MSP NDs with flipped t-SNARE cells, we tested the role of the transmembrane domains of v-SNARE proteins [38,63]. We found modifications designed to disrupt putative interactions between v- and t-SNARE TMDs [64] resulted in much longer lifetimes, but also lower fusion rates. The two effects can compensate to some extent and result in nearly the same amount of calcium release from liposomes when the same mutations are tested in a bulk ND-liposome fusion assay [38].

With the pore diameter limited to ≲ 4 nm, MSP NDs are useful for mimicking the initial, small exocytotic fusion pores, but are not suitable to monitor larger pores. To study mechanisms contributing to pore dilation, we turned to larger, ~25 nm NLPs stabilized by a belt of apolipoprotein E (apoE) derivative, apoE422k [48,52]. These larger discs allow incorporation of a larger number of v-SNAREs per disc, and the pore size is not limited by the scaffold up to a diameter of ≳ 10 nm [35,37]. We systematically varied the v-SNARE copy number per NLP and measured the fusion rate and mean single-pore conductance [37]. We found that the fusion rate saturated above ~2 v-SNAREs per NLP face, whereas the mean single pore conductance increased sharply with increasing copy numbers up to ~15 copies per face, the maximum tested. These results showed that a fusion pore can be opened with only a few SNARE complexes, consistent with several previous estimates [36,40,65–68]. However, efficient pore dilation required cooperative action of many more SNAREs [37]. A simple explanation for this cooperativity is entropic forces generated by molecular crowding at the pore's waist [37].

Together, these studies suggest that ND-cell fusion pores induced by SNAREs alone tend to remain small (~1–2 nm diameter), with only transient excursions to diameters that are several nm. Pores flicker, fluctuate in size, and display a broad range of properties. Increasing SNARE copy numbers increases the mean single pore conductance up to at least 15 copies per disc face, but the rate at which pores open saturates rapidly at around 2 copies [37].

A limitation of the ND-cell fusion approach is that the lipid composition of the outer leaflet of the plasma membrane which is poor in acidic lipids does not reflect the physiologically relevant composition, which is that of the inner leaflet, rich in phosphatidylserine (PS), phosphatidylinositols, and other acidic lipids. The roles of such lipids can be tested by exogenous addition of short-chain versions to the outer leaflet. When fusion is driven by SNAREs alone, lipid composition has a limited effect (except for cholesterol [39,69]), but certain lipids such as phosphatidylinositol 4,5 bisphosphate ($PI(4,5)P_2$) play a crucial role during exocytosis, due to their interactions with other components of the fusion machinery such as the calcium sensor Synaptotagmin-1 [70,71]. Recent ND-cell fusion experiments indicate the calcium sensor Synaptotagmin-1 promotes pore dilation (at fixed SNARE copy number) in a calcium, SNARE, and PI(4,5)P2-dependent manner (Wu et al., in preparation).

2.3 Nanodisc-black lipid membrane (BLM) fusion

Bao et al. [41] used a BLM as the target membrane for fusion with v-SNARE reconstituted, ~13 nm diameter MSP NDs (Fig. 2D). BLMs are suspended bilayers that are commonly used in single ion channel studies [72]. The bilayer was prepared by painting a solution of lipids dissolved in n-decane over a ~150 μm orifice in a thin hydrophobic partition separating two chambers. Bao et al. loaded a large, non-limiting density of t-SNAREs (0.4/μm^2) into the BLM via fusion of t-SNARE liposomes with BLMs. Both had a lipid composition that allowed spontaneous fusion (75% phosphatidylethanolamine (PE) and 25% phosphatidylglycerol (PG)). After rinsing the excess t-SNARE liposomes, v-SNARE NDs were introduced into one chamber and currents across the BLM were monitored under voltage-clamp.

Surprisingly most pores had stable, ion channel-like conductances [41], in contrast to earlier work by us using 16–17 nm MSP NDs fusing with engineered cells [38] (Fig. 2). With increasing v-SNARE copies per disc, open-pore conductance, pore lifetime, and pore open probability increased, consistent with previous work [37]. Pore size estimates ranged from ~0.5 to 3 nm diameter, consistent with the maximum size a pore can reach in a 13 nm ND. Pore lifetimes were extremely long, many pores lasting minutes, and remaining open during the entire pore lifetime for the discs carrying the largest number of v-SNAREs (3–4 per face). Addition of increasing amounts of the cytoplasmic domain of Syb2 (cd-Syb2), but not BSA, resulted in increased flickering and a corresponding decrease in pore open probability. Similarly, truncating the C-terminal 20 residues of SNAP25, mimicking the cleavage product of BoNT/A, led to increased transient pore closures (flickers). These findings led the authors to propose that pore size is determined by SNARE copy numbers, with flickering controlled mainly by dynamic trans-SNARE interactions at the membrane proximal end. Since they are under load, it is possible that membrane-embedded v- and t-SNAREs interacting in *trans* partially zip and unzip dynamically, rendering the already engaged v-SNAREs susceptible to displacement by soluble cd-Syb2. However, given that cd-Syb2 encompassed the entire cytoplasmic domain of Syb2 and that formation of a single v-/t-SNARE (cytoplasmic) complex releases 65 kT free energy [73], it is baffling that cd-Syb2 binding to t-SNAREs in the BLM would be reversible, as suggested by continued pore flickering for minutes.

Bao et al. [41] also showed that decreasing SNARE copy numbers in neuronal cultures lead to slower miniature post-synaptic currents in cortical neuronal cultures, consistent with smaller pores limiting neurotransmitter release when only a few SNAREs complexes are available for fusion. Previous, less direct measurements also support the same idea [74,75].

A striking difference between the ND-cell [38] and ND-BLM [41] experiments using 13–15 nm NDs is that small fusion pores in the latter have well-defined conductance levels similar to ion-channels (Fig. 2D), whereas such stable pores are rare in the former (Fig. 2C and Fig. 3A). Both assays have drawbacks and it is difficult to say which represents the physiological situation better. In the ND-BLM experiments, BLMs were formed using n-decane, residual amounts of which remain in the bilayer [72,76]. How residual solvent affects fusion rates and pore dynamics is not known, but it can dramatically affect membrane dynamics [77]. The lipid composition used was far from physiological (75% PE and 30% PG). Finally, even simple bilayer pores in BLMs can have ion-channel-like stable conductances and flickers in the absence of any protein [78]. As for the ND-cell experiments, the composition of the outer plasma membrane is very different than that of the inner leaflet which a vesicle normally encounters during exocytosis. During ND-cell fusion, we actually do find some pores that have relatively stable conductances, but many of these are excluded from analysis because their amplitude/duration is lower than the set threshold [38,62]. Channel-like pores that conform to the cutoff to be included in analysis are rare and the conductances are not uniform for a given condition (Fig. 3A). We also cannot exclude the possibility that rare channel-like currents in the ND-cell fusion assay are actually due to ion channels despite inclusion of channel-inhibiting drugs. Finally, a channel-like initial pore may escape detection if it is short lived ($\lesssim$ 1 ms). Interestingly, when larger, 50 nm NDs were used by

Bao et al., some pores dilated, and currents fluctuated [41], resulting in current profiles that looked qualitatively similar to those found in the ND-cell fusion assay [37].

Given the important differences in the target membranes used, and the different nanodisc preparations, it is not surprising that observations be somewhat different between ND-cell [38] and ND-BLM [41] studies. Indeed, influenza hemagglutinin (HA)-mediated fusion pores display different characteristics depending on the target membrane. When cells expressing the influenza fusogen hemagglutinin (HA) on their surfaces [79] are fused to a BLM, channel-like pores flicker for 10s of seconds before further expansion [80]. By contrast, when the same cells are fused to a red blood cell, pores flicker less; instead they rapidly reach a conductance of 400–700 pS and fluctuate for seconds before dilating further [81].

It is important to have alternative experimental approaches, as they permit judging which observations are assay-specific, and which are general.

3. FUSION PORE PROPERTIES MEASURED DURING EXOCYTOSIS

How do the recent single-pore measurements of membrane fusion (so far driven only by SNAREs) compare with exocytotic fusion pore measurements? Different approaches to detect fusion pores during exocytosis from neuroendocrine cells have resulted in remarkably different estimates of fusion pore properties. I briefly review the most relevant approaches below, emphasizing the strengths and limitations of each, and suggest how apparently disparate observations can be reconciled.

3.1. Time-resolved admittance measurements

Time-resolved admittance measurements provide the most direct monitoring of fusion pores during exocytosis for extended periods of time [82], but only a narrow window of pore sizes centered around the admittance of the fusing vesicle (dominated by its capacitive admittance, ωC_V, where ω is the driving frequency and C_V is the vesicle capacitance) can be detected, depending on instrumental parameters and overall noise [83,84]. The method relies on the fact that membrane capacitance is proportional to membrane area [82]. The cell-attached configuration [60] allows the lowest noise [84], since only a small area of the plasma membrane is probed. A sinusoidally varying potential (typically 10–40 kHz for cell-attached measurements) is added atop a holding potential. Currents that are in- and out-of-phase with the driving sinusoidal voltage are monitored using phase-sensitive (lock-in) detection. The in-phase currents reflect resistive elements in the circuit, whereas capacitive elements introduce phase shifts. The capacitance and conductance (1/resistance) of the patch are calculated from the in- and out-of-phase components of the current by assuming that fusion of a vesicle introduces a new capacitance in parallel with the initial, pre-fusion patch capacitance (Fig. 4.B). If the fusion pore is sufficiently small, it presents significant resistance to the passage of ions and prevents complete charging and discharging of the capacitance of the newly fused vesicle membrane with each sinusoid cycle. When this condition is met, the pore resistance (or its inverse, the pore conductance) can be calculated assuming a resistor in series with the vesicle capacitance [22,82].

When the pore dilates beyond a certain limit that depends on the driving frequency, the noise level, and vesicle capacitance, pore resistance becomes too small to be detected, and its inverse, the conductance, diverges [83,84] (Fig. 4B, 2 red curve). Thus, different lock-in driving frequencies probe different fusion pore size windows for a given vesicle size. Using higher driving frequencies favors detection of larger pores [84]. For example, He et al. [85] found mean fusion pore conductance G_p = 66 ± 7 pS and 146 ± 24 pS for 15–17% of synaptic vesicles displaying capacitance flickers at Calyx synapses using driving frequencies of 20 and 90 kHz, respectively. Pore conductance could not be detected for the rest of flickering pores, implying $G_p \gtrsim 288$ pS, the estimated upper limit of detection in that study (where most vesicles were ~50 nm in diameter, with 80 aF capacitance). Mast cells of the beige mouse have large, ~2–3 μm secretory granules ($C_v \approx 120 – 300$ fF) and are thus better suited to monitoring larger pore conductances. Curran et al. used a range of driving frequencies (0.3–3.2 kHz, whole-cell recordings) to extend the range of detectable fusion pore conductances to 0.2–100 nS [83]. They found most pores expanded rapidly to 0.6–20 nS conductance (corresponding to 3–15 nm diameter, assuming pore length=15 nm). Some pores displayed one or more semi-stable conductance levels within that range, for up to 15 s. For chromaffin cells which are widely used for studying mechanisms of exocytosis, granules are 200–300 nm in diameter ($C_v \approx$ 1–3 fF) and typically measurable $G_p < 1 – 2$ nS, corresponding to $2r_p <$ 2–5 nm (for a 15 nm long pore) [86].

Although the technical limitations mentioned above are well-known [83–85], it is often assumed that a pore that expands beyond the detectable size will keep expanding until the vesicle collapses into the plasma membrane. However, many other possibilities exist that would be consistent with the same admittance recordings, as illustrated in Fig. 4A, B.

The lifetime of the initial, small pore conductance before further pore dilation is typically 20–90 ms in chromaffin cells [87,88], 10–300 ms in the Calyx synapse [85], up to seconds in peritoneal mast cells [89], ~0.3 s and ~0.6 s for for microvesicle and dense core vesicle exocytosis in posterior pituitary nerve terminals [90], and often, but not always [89], correlates well with the lifetime of the amperometric PSF in simultaneous amperometry and admittance measurements [91]. For pores that do not expand beyond the detectable conductance range, pore conductance can fluctuate around a mean value for up to seconds in chromaffin cells [91]. Around 20% and 40% of human and mouse pancreatic beta cells, respectively, display exceptionally stable fusion pores lasting minutes [92].

The lifetime of a fusion pore can be estimated from the capacitance trace even if the pore conductance becomes too large to be detected (Fig. 4B, 4). Such capacitance flickers last ~0.5 s in chromaffin cells [86] or ~0.3 s in Calyx synapses [85]. These are underestimates, because it is difficult to follow the fate of the same pore for an extended period of time when capacitance steps from different fusion events may start overlapping. Analysis is often limited to 1–2 s from the initial up-step [85,90]. It is usually assumed that successive up and down capacitance steps of similar size represent flickering of the same pore [85,90]. This is a good assumption; however, membrane can flow between the fused vesicle and the plasma membrane, in either direction [33,93,94]. Such uneven capacitance steps (Fig. 4B) are not always included in analysis.

In summary, admittance measurements indicate fusion pore conductance can expand beyond the detection range (typically 2–5 nm diameter) within 1–1000 ms. For pore conductances that remain within the detection window, G_p can sometimes fluctuate around one or more semi-stable plateau values [83,91], or be stable for minutes [92]. Capacitance flickers suggest lifetimes of flickering pores can last ~0.3–0.5 s or longer in neurons [85] and chromaffin cells [86]. Since pore conductance cannot be detected for many such flickers, pores that dilate rapidly beyond the detection range of G_p must be able to close transiently (flicker) and eventually reseal [86,90].

3.2. Electrochemical detection of fusion pores

Many secreted compounds, such as catecholamines, can be oxidized at diffusion-controlled rates at the surface of a carbon fiber electrode held at the appropriate potential and placed near the secretory cell [95,96]. The oxidation current that is generated is proportional to the flux of cargo reaching the electrode surface.

Different modes of exocytosis have been detected using amperometry. Chromaffin cells stimulated at a low frequency (0.5 Hz) mimicking basal conditions secrete catecholamines in a way that produces mostly small amplitude, ~100 ms wide amperometric spikes, consistent with release through pores that are too small to release larger neuropeptide cargo [31] ((Fig. 4C, 1). The time integral of the current trace ($\propto$ number of oxidized cargo) indicated only a small fraction of vesicle contents was released during such events. In some cases, pore flickering could clearly be detected by a rapid succession of amperometric spikes that continuously decreased in amplitude [31] (each flicker releases a fraction of the cargo, leaving a smaller amount for the subsequent pore opening) (Fig. 4C, 1). Successively decreasing amperometric spikes consistent with release through a flickering pore were also detected in cultures of dopaminergic neurons but had a much higher flicker rate [28]. By contrast, high frequency stimulation (15 Hz) mimicking acute stress condition elicited mostly amperometric traces that were much larger in amplitude and much shorter in duration (~10 ms) [31]. The time integral of the current indicated release of the majority, or all, vesicular catecholamines. A characteristic feature, a pre-spike foot (PSF) signal, preceded ~30% of spikes (Fig. 4C, 4). The PSF [96,97] reflects release through the initial, small-sized fusion pore, as shown by simultaneous admittance and amperometry measurements [86,91,98].

In very low-noise recordings, a small-amplitude, short-lived signal called stand-alone feet (SAF) can be detected by amperometry [97,99] (Fig. 4C, 2). Simultaneous admittance and amperometry measurements indicate SAF is produced from a small pore that reseals without ever expanding to give rise to a spike [86,100]. SAF last ~20 ms in PC12 cells [99] and ~100 ms in bovine chromaffin cells [97].

The lifetime of the PSF signal is typically ~1–2 ms in PC12 [101], ~3 ms in mouse chromaffin cells [88] and ~50 ms in bovine chromaffin cells [97]. This is much shorter than the pore lifetimes reported by admittance measurements that are based on capacitance steps (~0.3–0.5 s, see section 3.1). This discrepancy is due to the different processes detected by amperometric PSF and capacitance steps. The latter does not depend on pore size, yet it is often assumed that a pore that flickers must remain small, even if pore conductance is not

detectable. This assumption is not always correct [33,86] (see section 3.4). By contrast, the PSF reflects release through the initial, ~1 nm diameter pore [96,97], and correlates well with the conductance of small pores detectable in simultaneous amperometry and admittance measurements [91,100,102]. Thus, it is more appropriate to compare the PSF signal with measurements of initial pore conductance when this parameter is detectable, even though the two approaches are not necessarily tuned to detect the same pore size range and have different temporal resolutions [88].

Spike parameters have been analyzed in detail in order to extract information about the kinetics and extent of catecholamine release [102–104]. Because many neurotransmitters and hormones are charged and the granule matrix of many neuroendocrine cells contains highly charged polyelectrolytes [105], release may be governed by an ion-exchange mechanism characterized by an electrodiffusion process [102,106,107]. Ion exchange can also lead to the hydration and swelling of the granule matrix, in particular of mast cell granules [20,83,102], which may contribute to pore expansion at late stages [83,108,109]. The extent to which electrodiffusion governs release is expected to vary among different cell types since the granule contents can be very different. Once the small, charged small molecule cargo (e.g. catecholamine) escapes the matrix and through the pore, it still needs to diffuse through a certain distance to reach the electrode surface. This diffusion will broaden signals, with stronger broadening for release at more distant sites [103,104]. Sometimes a maximum rise time or width at half height of the spike is chosen as a cutoff to exclude spikes that may be broadened due to release occurring at distant sites [110]. But these cutoffs will also exclude events for which release does occur slowly, e.g. due to a small, flickering pore, without serious diffusive broadening. Finally, the catecholamine flux at the electrode surface depends on the concentration of catecholamines in the fusing vesicle, but individual vesicles may contain different concentrations of cargo [110–112].

The considerations above make it difficult to quantitatively relate the oxidation current profile to release kinetics. Yet, it is often assumed that spikes correspond to full-fusion events in which the pore dilates irreversibly until the vesicle collapses into the plasma membrane. This is not necessarily so: like the pore conductance deduced from admittance, amperometric spike kinetics are not sensitive to pore size beyond a certain cutoff, particularly for the release of small cargo detected by amperometry [113], and slow release events may be missed due to cutoffs designed to eliminate signals broadened by diffusion [110]. An alternative scenario is that the initial small pore (~1 nm diameter, detected as the PSF signal) can expand to a larger size, without fully collapsing into the plasma membrane, giving rise to a large spike (Fig. 4C, 4). Because flux through the pore increases with pore area, a moderate expansion of the initial pore by a few nm translates to a large increase in cargo efflux and the amperometric signal. Indeed, modeling suggests amperometric spike profiles cannot distinguish the fate of the pore after the initial dilation: nearly the same signal would be produced by a moderately large pore (~20–30 nm) that remains open or a pore that collapses completely [114] (Fig. 4C, 4). In addition, like any efflux measurement, once a vesicle is emptied of all probe (catecholamines for chromaffin or PC12 cell exocytosis) no further information can be drawn regarding the subsequent stages of fusion [86]. Only if the pore reverts to a small enough size limiting efflux and/or reseals *before* all probes are emptied can the consequences be detected. During secretion from PC12 cells,

Mellander et al. [115] detected post-spike features that were consistent with a pore reverting to a small size (producing a plateau after a large amperometric spike) that abruptly closed (the plateau rapidly returning to the baseline) (Fig. 4C, 3). The authors argued that due to the difficulties in detecting such post-spike feet, they were severely undercounted [115]. Events with post-spike feet were called extended kiss-and-run events. Consistent with the idea that even some oxidation current profiles without detectable post-spike feet may be due to partial release events, Li et al. found only ~65% of the catecholamine cargo of a granule is released during exocytosis in PC12 cells [116]. These and other considerations lead Ren et al. [113] to propose that pores can dilate to relatively large sizes (20–30 nm) and reseal, in what they termed as “open-close” exocytosis.

Using simultaneous amperometry and admittance measurements, Ales et al. [86] found some amperometric spikes started rising concurrently with a capacitance up-step, but decayed much earlier (up to ~1 s) than the capacitance down-step, demonstrating pore closure cannot be detected using amperometry after the vesicle empties its catecholamines. Unexpectedly, in other events, the capacitance down-step, indicating pore closure, occurred shortly after the onset of the amperometric spike. These events indicate a pore can briefly expand to a large enough size allowing rapid catecholamine release that gives rise to an amperometric spike, but can close back soon thereafter.

In summary, amperometry can detect the initial, ~1–2 nm sized fusion pore as a PSF signal, and the subsequent expansion of the pore to a larger size producing a spike. The spike-producing larger pore can be small compared to vesicle size, or can dilate until full-collapse. Unless the pore reverts to a small size and/or reseals before the oxidizable small molecule cargo is emptied, no information regarding the fate of the pore beyond the initial expansion can be extracted reliably.

3.3. Total internal reflection fluorescence microscopy (TIRFM)

Like amperometry, TIRFM studies have often been efflux measurement, but the labeled protein (hence the probe size and other properties) can be selected. Relatively small probes, such as neuropeptide-Y (NPY, ~5 nm×2.5 nm×1.5 nm [117]) fused to a fluorescent protein, are usually released from the vesicular lumen of neuroendocrine cells within 0.1–1 s upon fusion with the plasma membrane [118–121] (Fig. 4D). This release time is longer than the amperometric PSF lifetimes, or even the release time (width at half-height of amperometric spike) of the entire catecholamine content upon strong stimulation (Fig. 4C), measured in the same cell types. This suggests the pore restricts release of small protein cargo more severely than that of small catecholamines. Nevertheless, probes such as NPY fused to a fluorescent protein that leave the fused granule rapidly are not very useful in determining the fate of the fusion pore and the granule ghost after fusion.

The fate of the granule after fusion is best probed using cargo that cannot be released rapidly, because, like any efflux measurement (including amperometry), once the probe leaves the fused vesicle, no information can be obtained regarding the subsequent fate of the pore or the vesicle. Several TIRFM studies identified cargo that remained at the fusion site for 10s of seconds or minutes, such as phogrin (a ~60 kDa granule membrane protein) [120] or BDNF (~27 kDa as a dimer, ~8 nm) [18]. Fusion of such probes (in the case of membrane

proteins the lumenal end) to a pH-sensitive fluorescent protein such as EGFP or pHluorin allows probing the fate of the fusion pore and the vesicle membrane. Fluorescence brightens rapidly upon fusion, due to neutralization of the normally acidic pH of the granule lumen by proton efflux through the fusion pore [122]. In contrast to rapidly released cargo, the fluorescence of EGFP-phogrin [120,121] or BDNF-EGFP [18] decayed slowly in 5–10 s, consistent with resealing of the fusion pore and subsequent re-acidification (Fig. 4D, right). To test if pores had re-sealed, ammonium chloride was applied externally to collapse the proton gradient [18,120]. This re-brightened previously fused granules to the same level as before fusion, indicating the dimming was due to acidification and not to loss of labeled cargo [18,120] (Fig. 4D). Expression of cytosolic CFP resulted in dark spots occupied by granules (marked by another probe), as CFP was excluded from the granular volume [120]. This exclusion persisted for at least ~1 min after granule exocytosis, indicating granules retained their Ω-shape after fusion [120].

Evidence for persistence of granule shape after fusion for ≳ 10 s was provided in other studies. Tran et al. monitored release of NPY-EGFP from human neuroendocrine cell line BON in the presence of an extracellular florescent 3 kDa dextran [119]. Dextran fluorescence was weak in the zone of cell-substrate adhesion, because this space is only ~20 nm thick. Shortly after, or concurrently with, release of NPY-EGFP from the granule lumen upon fusion, a dextran spot appeared and persisted for 5–15 s [119]. Anantharam et al. [123] used polarized TIRFM to monitor plasma membrane deformations, by detecting fluorescence of an externally added membrane dye with a preferred orientation of its excitation dipole with respect to the membrane. In chromaffin cells, granule shape was retained for up to tens of seconds [123]. Llobet et al. [124] used interference reflection microscopy and Shin and Gillis [125] ion scanning microscopy to detect long-lived plasma membrane invaginations at cell surfaces associated with exocytosis.

Retention of vesicular shape after fusion allows endocytosis of the fused vesicle en bloc, termed “cavicapture” [120,121,126]. It also allows fusion of a vesicle located deeper into the cytosol with the ghost of the newly fused vesicle, a process termed sequential fusion [127–129] which is challenging to detect unambiguously using TIRFM [119].

Together, TIRFM and other imaging studies in neuroendocrine cells have suggested that: 1) most secretory granules retain their shape after fusion for 1–100 s; 2) fusion pores can reseal during this time; 3) retention of granule shape after fusion allows retrieval of the ghost granule membrane en bloc, as well as other processes such as sequential fusion.

3.4. Dye influx measurements

When a fluorescent dye is dissolved in the bath solution, bath fluorescence is very high, whereas a cell, or cluster of cells, appears dark as its volume excludes the dye. The extracellular dye can enter the vesicular lumen upon exocytosis of a vesicle, manifested as a small bright spot appearing near the plasma membrane [128–131] (Fig. 4E). For these measurements to be successful, dye entry into the fused vesicle’s lumen and image acquisition must be faster than vesicle collapse. Indeed, vesicular shape is typically retained for many seconds [128–131]. This opens the possibility of long-lived, dynamic pores, but it is not possible to tell directly pore lifetime from such studies. Information about the state of

the pore has been obtained by periodically photobleaching fusion sites marked by dye uptake and monitoring if the bleached fluorescence can be recovered by dye exchange with the bath [130,131]. Such measurements indicated long-lived fusion pores (~11 min) during zymogen granule exocytosis in pancreatic acinar cells [130]. Similarly, cycles of dye perifusion, stimulation, washing, and re-perifusion indicated pore lifetimes of up to minutes in PC12 cells [129].

A general difficulty in dye influx experiments is to pinpoint the timing of pore closure. A major breakthrough was achieved in Ling-Gang Wu's laboratory by developing an elegant and simple approach: simultaneous use of a pair of extracellular tracer dyes, one to probe vesicle shape after exocytosis, and the other, excited at high power, to probe the state of the fusion pore via bleaching [32]. Stimulation of a chromaffin cell is achieved using whole-cell voltage-clamp. Upon exocytosis, both dyes enter the lumen of a fused vesicle through the fusion pore. One of the dyes is excited at low power (vesicle probe), the other at high power (pore probe). The intensity of the former depends on vesicle size and shape, but not pore dynamics. The latter probes the status of the fusion pore: if the pore closes, the bleached dye cannot exchange with unbleached dye in the bath and the fluorescence intensity starts decreasing rapidly ($\tau_{bleach} \approx 2.9$ s). If the pore re-opens after a transient closure, the fluorescence intensity recovers. Later experiments included two-color STED super-resolution imaging of an extracellular tracer dye to monitor pore state as before and a membrane probe that bound to fused vesicle ghosts after fusion (phospholipase C δ PH domain, binds PtdIns(4,5)P_2 which diffuses onto the granule's cytoplasmic leaflet after fusion) [33]. The membrane probe allowed direct measurement of pore sizes > 60 nm, the STED resolution.

Overall, these studies led to a picture in which fusion pores have a surprisingly diverse spectrum of fates. The initial, ~1–60 nm diameter pore (probe size $\lesssim 2\ r_p \lesssim$ STED resolution) can dilate rapidly (within ~30–50 ms, one imaging frame) or after a variable delay (0.5–4 s) to a diameter $\gtrsim$ 60 nm. Pore sizes ranged from those detectable by influx of bath tracer (Atto or Alexa dyes), to nearly granule size (~600 nm for the largest granules). A pore could stay open for >30 s, retain its size, or swell or shrink. Some pores closed, after any of these fates, with a very broad distribution of pore lifetimes. Surprisingly, even the largest pores were able to revert to small sizes and reseal, sometimes rapidly. Resealing of Ω-shaped pores could account for both the rapid and slow endocytosis described earlier for chromaffin cells [32]. That is, pore dynamics determined endocytosis kinetics. Some pore openings and closings went through hemifusion/hemi-fission intermediates that could also be visualized directly [132]. Pore opening was found to be promoted by membrane tension (mainly controlled by F-actin polymerization [34]) and closure by dynamin and high calcium [32,33].

A limitation of the dye influx/bleaching approach is that it can probe pore flickering on the several seconds timescale, even if images can be acquired at a much faster rate, because faster pore dynamics would be filtered by the bleaching time, on the order of ~3 s.

4. DISCUSSION: A UNIFIED PICTURE OF THE FUSION PORE

4.1 The same fusion pathway can lead to very different pore lifetime and size estimates, depending on the experimental approach

Reported exocytotic fusion pore properties depend strongly on the method used. In neuroendocrine cells, pore lifetimes estimated using different methods range ~0.1–0.5 s for capacitance (in some cases pores lasting > 5 min could be observed in pancreatic β-cells [92]), 1–50 ms from amperometry, and ~1–100 s from imaging. Some of these differences are doubtless due to differences in cell types which have distinct physiology. In addition, different stimulation protocols lead to different modes of fusion for the same cell type [31,133]. Finally, differences may arise from different perturbations that are inevitable for every approach. For example, cell-attached recordings perturb membrane tension and the cytoskeleton strongly [134,135] and TIRFM detects release only from the substrate-attached side of a cell. Although these perturbations may affect exocytosis to some degree, secretion [124] and pore properties [136–138] do not vary dramatically between the substrate-attached and bath-exposed sides of a cell (but see [139]).

Even with the same cell type studied in the same laboratory, however, different approaches often result in dramatic differences in fusion pore lifetime estimates [88] (pore sizes are more difficult to estimate using multiple approaches). Thus, it is likely that the remarkable differences in pore properties reported by various approaches are at least partially due to the fact that every method probes a different length and time scale during the fusion process. Figure 4A depicts fusion pore/vesicle fates that have been reported to date in neuroendocrine cells by direct observation using one or more approaches. In addition, hemifusion/hemifission intermediates have also been detected, but those would be silent in admittance, amperometry, and dye influx-efflux measurements [132]). Interestingly, although previous interpretations may have been different at times, data from different approaches are actually consistent. To illustrate how the same sequence would be reported (and perhaps interpreted) differently, imagine a fusion pore first opens to a small diameter (~1–2 nm) for ~10 ms (Fig. 4A, transition a→b), then expands to ~10–20 nm (Fig. 4A, state c) for ~5 s before resealing (back to state a). Depending on the driving frequency and signal-to-noise ratio, admittance might pick up the initial pore conductance and report both a rapid capacitance increase and a diverging conductance following a ~ 10 ms plateau (Fig. 4B, traces labeled 2, a→b→c), or the pore conductance might be undetectable (Fig. 4B, 3). If the pore flickers from its ~10 nm wide state, admittance would report this as capacitance flickers (Fig. 4B, 4), but conductance would be undetectable for such a large pore. The capacitance flickers would not be analyzed beyond 1–2 s, since the identity of the fused vesicle would be less certain when considering longer periods. Thus, capacitance would report a 1–2 s pore lifetime (depending on the cutoff used) and conductance a ~10 ms initial small pore.

For the same process, amperometry would report a trace such as the one labeled 4 in Fig. 4C, with the PSF lasting ~10 ms (the lifetime of state b). The reported fusion pore lifetime would be 10 ms. The rise of the spike would reflect a convolution of pore dilation (from state b to c), dissociation of the catecholamines from the vesicular matrix, and diffusion to the electrode surface. The decay of the spike would reflect dissociation of catecholamines

from the granular matrix and diffusion, but would not be sensitive to pore size, nor lifetime. The catecholamines would be emptied within 5–10 ms through the 10–20 nm pore and no further signal would be detected from this event, even though our hypothetical pore remained open for 5 s.

For the same sequence of events, TIRFM would report a ~0.1 s wide spike if NPY-pHluorin fluorescence is monitored (Fig. 4D left trace), limited by NPY-pHluorin release rate. If a larger cargo molecule, or one that interacts with the matrix or the vesicle membrane is labeled, release would be much slower, and perhaps only partial (Fig. 4D, right), reflecting release, resealing, and re-acidification. The pore lifetime (and size) would be very uncertain, especially for smaller cargo.

A single-color dye influx imaging experiment would report a step-like increase in fluorescence at a spot near the cell border (Fig. 4E, right, top trace) for the same fusion event, but pore lifetime would not be detected. Only the 2-color dye influx experiment would be able to detect the true pore lifetime (Fig. 4E, right, both traces), however, it would likely miss pore flickers, because signals are low-pass filtered with a cutoff frequency that corresponds to the inverse bleaching time of the strongly illuminated dye (~3 s). The initial, short-lived small pore (state b) would also be missed, because image acquisition period would typically be slower than the ~10 ms lifetime of state b.

4.2 Fusion pore, kiss-and-run, kiss-and-linger, cavicapture, porocytosis, kiss-and-coat, extended kiss-and-run, open-close exocytosis, etc.: distinct processes or the same process viewed through different glasses?

Since the first detection of exocytotic fusion pores in the early 70's by electron microscopy [140,141], and in the late 80's using electrophysiology [19,20], the field has been rife with debates regarding the composition and the fate of the fusion pore [26,142]. There is some confusion and almost dogmatic (mis)conceptions in the field surrounding fusion pores. This stems from a combination of 1) method-based definitions of fusion pores, with often creative terms such as "fusion pore", "cavicapture", "kiss & coat", "kiss and run", "open-close exocytosis", 2) often unjustified speculations regarding phases of the fusion process that cannot be detected by a given method, 3) exceptionally large intrinsic variability in fusion pore properties themselves, and 4) ambiguities in interpreting more challenging and indirect measurements of fusion pore properties in synaptic vesicle exocytosis. I propose to define "fusion pore" as any pore connecting two fusing membranes with a size smaller than the vesicle diameter, $r_{pore} < r_{ves}$. This is a method-independent definition. When information about fusion pores are reported, authors should clearly mention the limits of their detection window (even very approximately) and avoid speculating about phases of the fusion process that cannot be detected by their approach.

Pore conductances increasing beyond detection range in admittance measurements and amperometric foot currents followed by large amperometric spikes have been traditionally interpreted as signatures of pores irreversibly dilating, leading to complete vesicle collapse, despite any lack of justification (sections 3.1–3.2). In fact, such measurements are equally consistent with imaging studies which suggested much longer pore lifetimes and vesicles

rarely collapsing (sections 3.3–3.4), if we recognize the different length- and time-scales probed by electrical approaches vs. imaging studies.

An important question that emerges is whether the initial, 1–3 nm diameter fusion pore, detectable as an amperometric PSF (or in some cases as SAF, section 3.2) or with a measurable conductance in admittance experiments with 0.1–10 ms resolution (section 3.1) represents the initial stages of the same process that is probed in imaging studies that are sensitive to larger pores (>60 nm for direct visualization) and longer lifetimes (>s) (sections 3.3–4). In other words, do the initial small fusion pore and one that is dilated to larger sizes represent two distinct modes of fusion and endocytosis, or are both part of the same process monitored by methods that can either detect the initial ~1 s with high resolution or the later stages with poor resolution?

There is no clear answer to this question at the moment, and likely will not be until the entire fusion process can be monitored with good time resolution and sensitivity or conditions are found that dramatically stabilize one state or another. Arguments favoring the initial pore representing a distinct state include the following. 1) The initial small pore may be expected to reflect the pre-fusion supramolecular arrangement that just led to fusion. In particular, a channel-like initial pore structure [19,21,55], a protein scaffold [23], or a ring-like pre-fusion arrangement of the fusion machinery [143] are all expected to have their mark on the properties of the initial pore, until such a structure dissociates. 2) The composition of the initial pore is expected to change as the pore dilates. 3) After rapid dilation to a 100–500 pS conductance, some pores display a semi-stable conductance for some period before further dilation or resealing, suggesting a protein scaffold stabilizing the pore structure. 4) Mutagenesis or overexpression of components of the fusion machinery alter the properties of the initial pore [55,99,144–148]. Counter-arguments are also compelling: 1) The conductance and lifetime of the initial pore is highly variable and dependent on instrumental parameters. If the initial pore is indeed stabilized by a protein scaffold or channel-like structure, either the stoichiometry must be highly variable, and/or such a structure must be very short-lived. 2) When admittance parameters are tuned to detect larger pores, they are also found to display semi-stable conductances (~6 nm in mouse pancreatic beta cells [92] or ~5–25 nm in beige mouse mast cells [83]), although larger pores may be stabilized by a different mechanism.

4.3 Comparison with properties of fusion pores in nanodisc assays

Understanding properties of exocytotic fusion pores requires assays with biochemically defined components that are sensitive to single pores. In addition, the method should be able to probe pore dynamics across a large pore size range, with sub-ms time resolution. Nanodisc-based measurements of single pore conductances possess these qualities [37,38,41]. Because direct currents are monitored, the dynamic range of the measurements is broad. The smallest conductance that can be measured at a given bandwidth is limited by signal-to-noise (the same limitations apply to single-channel measurements). For the largest conductance, amplifier saturation sets the limit.

So far ND-based single fusion pore measurements included only SNARE proteins and looked at slow, calcium-independent fusion [35–38,40,41]. This is obviously not a good

mimic of the physiological situation, but the strength of a model system is that it allows isolating the role of a specific parameter or component. Thus, it is informative to compare results of this minimalistic system with properties of exocytotic fusion pores. Fusion pores in the ND-cell fusion assay are characterized by broadly distributed parameters. Pore conductances span the physical limits imposed by the configuration. Semi-stable conductance levels are sometimes observed, but the plateau values vary widely. Pores have long, exponentially distributed lifetimes, with a characteristic lifetime of 5–15 s, even when the ND size is not limiting for pore expansion [37,38]. These long lifetimes and the broad lifetime distributions are consistent with exocytotic fusion pore lifetimes estimated from imaging studies (section 3.3–3.4) and not far from those estimated from capacitance flickers (section 3.1). ND-BLM fusion pores are even longer lived [41]. It is possible that these broad lifetime distributions reflect intrinsic bilayer properties, which are modulated in the cell by dynamin, calcium, F-actin dynamics, and other components to adapt to the stimulation pattern and to the functions of different cell types.

A simple and general principle for modulation of pore size has emerged from ND-based fusion assays; that crowding at the pore waist should lead to larger pores. Engagement of larger SNARE copy numbers lead to larger pores in the ND-cell [37] and ND-BLM [41] single-pore assays, and in bulk ND-liposome fusion [35,36], as they do in neuroendocrine cells [41,75] or neurons [74]. Of course, there are many additional components present in cells, and these may also contribute to crowding around the pore, but it is reasonable to expect the number of additional components to scale with the number of SNAREs that are engaged at the fusion site.

The role of TMDs was also examined in ND-cell fusion experiments [38], but it is more difficult to extract a simple and general conclusion. The geometry of the SNARE complexes [38], the flexibility of the TMDs [149,150], TMD-TMD and TMD-lipid interactions were all invoked to explain effects of SNARE TMD mutations or substitutions in ND-cell fusion experiments, liposome-based assays, or in exocytosis. Details can be found in a recent review [63].

In the ND-cell fusion assay, the most likely pore size is ~1 nm diameter, which may reflect intrinsic bilayer mechanics since it is independent of SNARE copy numbers or ND size [37]. This size range is similar to the initial fusion pore sizes estimated from admittance and amperometry during exocytosis [22,82]. However, in the ND-cell fusion assay with only SNAREs driving fusion, this most likely size is sampled throughout the pore lifetime via large fluctuations in conductance [37,38]. By contrast, in many electrophysiological measurements a stable or semi-stable initial pore conductance is observed [83,90], consistent with the idea that a channel-like structure or a protein scaffold stabilizes the pore geometry. In the case of pancreatic β-cells, some pores display a surprisingly stable conductance for minutes [92]. It is possible that a pre-fusion scaffold [23,143] may stabilize the exocytotic fusion pore geometry, at least for the initial 1–10 ms that corresponds to pore conductance and amperometric PSF measurements.

4.4 Outstanding questions and outlook

ND-based fusion assays so far included only SNARE proteins, but a number of additional proteins are known to affect exocytotic fusion pores, most notably Synaptotagmin [99,101,151] and Complexin [147]. Thus, it is of great interest to include these and additional components of the exocytotic fusion machinery in future ND-based fusion pore assays to try to understand how they affect fusion pores. Inclusion of additional components of the fusion machinery in the ND-cell fusion assay may reveal factors that are needed to stabilize pore conductances, promoting pore dilation and resealing. We found that Synaptotagmin promotes pore dilation as mentioned in section 2.2; the mechanisms are being investigated actively.

A better understanding of mechanisms governing pore dynamics will also be useful in understanding synaptic vesicle release, as characterization of fusion pores that arise during synaptic vesicle fusion is technically challenging and direct observations are rare.

A tripartite complex composed of Synaptotagmin, Complexin, and SNAREs has been suggested to form the minimal machinery for rapid calcium-triggered fusion [14,152,153]. The time resolution of experiments in which these components have been used to reconstitute calcium-triggered exocytosis ranged from ~5 min [14] to ~200 ms [9]. By contrast, fast synchronous release lasts only a few ms in neurons [154]. Thus, it is unclear if the tripartite complex alone can recapitulate synchronous release. A major goal of ND-based fusion assays with sub-ms time resolution is to determine which components are needed to reconstitute synchronous release, and other, slower release modes [154]. In the longer term, it is likely these reconstitutions will contribute to our understanding of how calcium triggers fusion at the molecular level, a major unsolved question in the exocytosis field.

ACKNOWLEDGEMENTS

I am indebted to the members of my laboratory and many colleagues for stimulating discussions. The work in the Karatekin lab is supported by the National Institute of General Medical Sciences (grant R01GM108954), and a Kavli Foundation Neuroscience Scholar Award (to EK).

REFERENCES

[1]. Sudhof TC and Rothman JE (2009). Membrane Fusion: Grappling with SNARE and SM Proteins. Science 323, 474–477. [PubMed: 19164740]

[2]. Jahn R and Fasshauer D (2012). Molecular machines governing exocytosis of synaptic vesicles. Nature 490, 201–207. [PubMed: 23060190]

[3]. Neher E (2018). Neurosecretion: what can we learn from chromaffin cells. Pflugers Arch 470, 7–11. [PubMed: 28801866]

[4]. Rorsman P and Ashcroft FM (2018). Pancreatic beta-Cell Electrical Activity and Insulin Secretion: Of Mice and Men. Physiol Rev 98, 117–214. [PubMed: 29212789]

[5]. Brunger AT, Choi UB, Lai Y, Leitz J and Zhou Q (2018). Molecular Mechanisms of Fast Neurotransmitter Release. Annu Rev Biophys 47, 469–497. [PubMed: 29792815]

[6]. Takamori S et al. (2006). Molecular anatomy of a trafficking organelle. Cell 127, 831–46. [PubMed: 17110340]

[7]. Neher E (2006). A comparison between exocytic control mechanisms in adrenal chromaffin cells and a glutamatergic synapse. Pflugers Arch 453, 261–8. [PubMed: 17016737]

[8]. Rizo J and Xu J (2015). The Synaptic Vesicle Release Machinery. Annu Rev Biophys 44, 339–67. [PubMed: 26098518]

[9]. Lai Y et al. (2017). Molecular Mechanisms of Synaptic Vesicle Priming by Munc13 and Munc18. Neuron 95, 591–607 e10. [PubMed: 28772123]

[10]. Schiavo G, Benfenati F, Poulain B, Rossetto O, Polverino de Laureto P, DasGupta BR and Montecucco C (1992). Tetanus and botulinum-B neurotoxins block neurotransmitter release by proteolytic cleavage of synaptobrevin. Nature 359, 832–5. [PubMed: 1331807]

[11]. Weber T, Zemelman BV, McNew JA, Westermann B, Gmachl M, Parlati F, Sollner TH and Rothman JE (1998). SNAREpins: Minimal machinery for membrane fusion. Cell 92, 759–772. [PubMed: 9529252]

[12]. Sollner T, Whitehart SW, Brunner M, Erdjumentbromage H, Geromanos S, Tempst P and Rothman JE (1993). Snap Receptors Implicated in Vesicle Targeting and Fusion. Nature 362, 318–324. [PubMed: 8455717]

[13]. Sutton RB, Fasshauer D, Jahn R and Brunger AT (1998). Crystal structure of a SNARE complex involved in synaptic exocytosis at 2.4 A resolution. Nature 395, 347–53. [PubMed: 9759724]

[14]. Giraudo CG, Eng WS, Melia TJ and Rothman JE (2006). A clamping mechanism involved in SNARE-dependent exocytosis. Science 313, 676–680. [PubMed: 16794037]

[15]. Geppert M, Goda Y, Hammer RE, Li C, Rosahl TW, Stevens CF and Sudhof TC (1994). Synaptotagmin I: a major Ca2+ sensor for transmitter release at a central synapse. Cell 79, 717–27. [PubMed: 7954835]

[16]. Martens S, Kozlov MM and McMahon HT (2007). How synaptotagmin promotes membrane fusion. Science 316, 1205–8. [PubMed: 17478680]

[17]. Hui EF, Johnson CP, Yao J, Dunning FM and Chapman ER (2009). Synaptotagmin-Mediated Bending of the Target Membrane Is a Critical Step in Ca2+-Regulated Fusion. Cell 138, 709–721. [PubMed: 19703397]

[18]. Lynch KL, Gerona RR, Kielar DM, Martens S, McMahon HT and Martin TF (2008). Synaptotagmin-1 utilizes membrane bending and SNARE binding to drive fusion pore expansion. Mol Biol Cell 19, 5093–103. [PubMed: 18799625]

[19]. Breckenridge LJ and Almers W (1987). Currents through the Fusion Pore That Forms during Exocytosis of a Secretory Vesicle. Nature 328, 814–817. [PubMed: 2442614]

[20]. Zimmerberg J, Curran M, Cohen FS and Brodwick M (1987). Simultaneous Electrical and Optical Measurements Show That Membrane-Fusion Precedes Secretory Granule Swelling during Exocytosis of Beige Mouse Mast-Cells. Proceedings of the National Academy of Sciences of the United States of America 84, 1585–1589. [PubMed: 3470745]

[21]. Jackson MB and Chapman ER (2008). The fusion pores of Ca2+ -triggered exocytosis. Nat Struct Mol Biol 15, 684–9. [PubMed: 18596819]

[22]. Lindau M and de Toledo GA (2003). The fusion pore. Biochimica Et Biophysica Acta-Molecular Cell Research 1641, 167–173.

[23]. Monck JR and Fernandez JM (1996). The fusion pore and mechanisms of biological membrane fusion. Current Opinion in Cell Biology 8, 524–533. [PubMed: 8791451]

[24]. Wu LG, Hamid E, Shin W and Chiang HC (2014). Exocytosis and endocytosis: modes, functions, and coupling mechanisms. Annu Rev Physiol 76, 301–31. [PubMed: 24274740]

[25]. Lou X (2018). Sensing Exocytosis and Triggering Endocytosis at Synapses: Synaptic Vesicle Exocytosis-Endocytosis Coupling. Front Cell Neurosci 12, 66. [PubMed: 29593500]

[26]. Alabi AA and Tsien RW (2013). Perspectives on kiss-and-run: role in exocytosis, endocytosis, and neurotransmission. Annu Rev Physiol 75, 393–422. [PubMed: 23245563]

[27]. Lisman JE, Raghavachari S and Tsien RW (2007). The sequence of events that underlie quantal transmission at central glutamatergic synapses. Nat Rev Neurosci 8, 597–609. [PubMed: 17637801]

[28]. Staal RGW, Mosharov EV and Sulzer D (2004). Dopamine neurons release transmitter via a flickering fusion pore. Nature Neuroscience 7, 341–346. [PubMed: 14990933]

[29]. Collins SC et al. (2016). Increased Expression of the Diabetes Gene SOX4 Reduces Insulin Secretion by Impaired Fusion Pore Expansion. Diabetes 65, 1952–61. [PubMed: 26993066]

[30]. MacDonald PE, Braun M, Galvanovskis J and Rorsman P (2006). Release of small transmitters through kiss-and-run fusion pores in rat pancreatic beta cells. Cell Metab 4, 283–90. [PubMed: 17011501]

[31]. Fulop T, Radabaugh S and Smith C (2005). Activity-dependent differential transmitter release in mouse adrenal chromaffin cells. Journal of Neuroscience 25, 7324–7332. [PubMed: 16093382]

[32]. Chiang HC et al. (2014). Post-fusion structural changes and their roles in exocytosis and endocytosis of dense-core vesicles. Nat Commun 5, 3356. [PubMed: 24561832]

[33]. Shin W et al. (2018). Visualization of Membrane Pore in Live Cells Reveals a Dynamic-Pore Theory Governing Fusion and Endocytosis. Cell 173, 934–945 e12. [PubMed: 29606354]

[34]. Wen PJ et al. (2016). Actin dynamics provides membrane tension to merge fusing vesicles into the plasma membrane. Nat Commun 7, 12604. [PubMed: 27576662]

[35]. Bello OD, Auclair SM, Rothman JE and Krishnakumar SS (2016). Using ApoE Nanolipoprotein Particles To Analyze SNARE-Induced Fusion Pores. Langmuir 32, 3015–23. [PubMed: 26972604]

[36]. Shi L, Shen QT, Kiel A, Wang J, Wang HW, Melia TJ, Rothman JE and Pincet F (2012). SNARE Proteins: One to Fuse and Three to Keep the Nascent Fusion Pore Open. Science 335, 1355–1359. [PubMed: 22422984]

[37]. Wu Z, Bello OD, Thiyagarajan S, Auclair SM, Vennekate W, Krishnakumar SS, O'Shaughnessy B and Karatekin E (2017). Dilation of fusion pores by crowding of SNARE proteins. Elife 6

[38]. Wu Z, Auclair SM, Bello O, Vennekate W, Dudzinski NR, Krishnakumar SS and Karatekin E (2016). Nanodisc-cell fusion: control of fusion pore nucleation and lifetimes by SNARE protein transmembrane domains. Sci Rep 6, 27287. [PubMed: 27264104]

[39]. Stratton BS et al. (2016). Cholesterol Increases the Openness of SNARE-Mediated Flickering Fusion Pores. Biophys J 110, 1538–50. [PubMed: 27074679]

[40]. Bao H, Goldschen-Ohm M, Jeggle P, Chanda B, Edwardson JM and Chapman ER (2016). Exocytotic fusion pores are composed of both lipids and proteins. Nat Struct Mol Biol 23, 67–73. [PubMed: 26656855]

[41]. Bao H et al. (2018). Dynamics and number of trans-SNARE complexes determine nascent fusion pore properties. Nature 554, 260–263. [PubMed: 29420480]

[42]. Leckband D and Israelachvili J (2001). Intermolecular forces in biology. Q Rev Biophys 34, 105–267. [PubMed: 11771120]

[43]. Karatekin E, Sandre O, Guitouni H, Borghi N, Puech PH and Brochard-Wyart F (2003). Cascades of transient pores in giant vesicles: Line tension and transport. Biophysical Journal 84, 1734–1749. [PubMed: 12609875]

[44]. Puech PH, Borghi N, Karatekin E and Brochard-Wyart F (2003). Line thermodynamics: Adsorption at a membrane edge. Physical Review Letters 90

[45]. Saitoh A, Takiguchi K, Tanaka Y and Hotani H (1998). Opening-up of liposomal membranes by talin. Proc Natl Acad Sci U S A 95, 1026–31. [PubMed: 9448279]

[46]. McLean MA, Gregory MC and Sligar SG (2018). Nanodiscs: A Controlled Bilayer Surface for the Study of Membrane Proteins. Annu Rev Biophys

[47]. Denisov IG and Sligar SG (2017). Nanodiscs in Membrane Biochemistry and Biophysics. Chem Rev 117, 4669–4713. [PubMed: 28177242]

[48]. Chromy BA et al. (2007). Different apolipoproteins impact nanolipoprotein particle formation. J Am Chem Soc 129, 14348–54. [PubMed: 17963384]

[49]. Nasr ML et al. (2017). Covalently circularized nanodiscs for studying membrane proteins and viral entry. Nat Methods 14, 49–52. [PubMed: 27869813]

[50]. Dorr JM, Scheidelaar S, Koorengevel MC, Dominguez JJ, Schafer M, van Walree CA and Killian JA (2016). The styrene-maleic acid copolymer: a versatile tool in membrane research. Eur Biophys J 45, 3–21. [PubMed: 26639665]

[51]. Durr UH, Gildenberg M and Ramamoorthy A (2012). The magic of bicelles lights up membrane protein structure. Chem Rev 112, 6054–74. [PubMed: 22920148]

[52]. Blanchette CD et al. (2008). Quantifying size distributions of nanolipoprotein particles with single-particle analysis and molecular dynamic simulations. J Lipid Res 49, 1420–30. [PubMed: 18403317]

[53]. Lai Y, Diao J, Liu Y, Ishitsuka Y, Su Z, Schulten K, Ha T and Shin YK (2013). Fusion pore formation and expansion induced by Ca2+ and synaptotagmin 1. Proc Natl Acad Sci U S A 110, 1333–8. [PubMed: 23300284]

[54]. Bowen ME, Weninger K, Brunger AT and Chu S (2004). Single molecule observation of liposome-bilayer fusion thermally induced by soluble N-ethyl maleimide sensitive-factor attachment protein receptors (SNAREs). Biophysical Journal 87, 3569–3584. [PubMed: 15347585]

[55]. Han X, Wang CT, Bai JH, Chapman ER and Jackson MB (2004). Transmembrane segments of syntaxin line the fusion pore of Ca2+-triggered exocytosis. Science 304, 289–292. [PubMed: 15016962]

[56]. Hu C, Ahmed M, Melia TJ, Sollner TH, Mayer T and Rothman JE (2003). Fusion of cells by flipped SNAREs. Science 300, 1745–1749. [PubMed: 12805548]

[57]. Giraudo CG, Garcia-Diaz A, Eng WS, Chen YH, Hendrickson WA, Melia TJ and Rothman JE (2009). Alternative Zippering as an On-Off Switch for SNARE-Mediated Fusion. Science 323, 512–516. [PubMed: 19164750]

[58]. Krishnakumar SS, Kummel D, Jones SJ, Radoff DT, Reinisch KM and Rothman JE (2013). Conformational dynamics of calcium-triggered activation of fusion by synaptotagmin. Biophys J 105, 2507–16. [PubMed: 24314081]

[59]. Krishnakumar SS et al. (2011). A conformational switch in complexin is required for synaptotagmin to trigger synaptic fusion. Nat Struct Mol Biol 18, 934–40. [PubMed: 21785412]

[60]. Hamill OP, Marty A, Neher E, Sakmann B and Sigworth FJ (1981). Improved patch-clamp techniques for high-resolution current recording from cells and cell-free membrane patches. Pflugers Arch 391, 85–100. [PubMed: 6270629]

[61]. Sakmann B and Neher E (2009) Single-channel recording, Springer New York, NY.

[62]. Dudzinski NR, Wu Z and Karatekin E (2018) A Nanodisk-Cell Fusion Assay with Single-Pore Sensitivity and Sub-millisecond Time Resolution. In SNAREs: Methods and Protocols (Fratti R, ed.^eds). Springer Science+Business Media, LLC, part of Springer Nature

[63]. Wu Z, Thiyagarajan S, O'Shaughnessy B and Karatekin E (2017). Regulation of Exocytotic Fusion Pores by SNARE Protein Transmembrane Domains. Front Mol Neurosci 10, 315. [PubMed: 29066949]

[64]. Stein A, Weber G, Wahl MC and Jahn R (2009). Helical extension of the neuronal SNARE complex into the membrane. Nature 460, 525–U105. [PubMed: 19571812]

[65]. Karatekin E, Di Giovanni J, Iborra C, Coleman J, O'Shaughnessy B, Seagar M and Rothman JE (2010). A fast, single-vesicle fusion assay mimics physiological SNARE requirements. Proceedings of the National Academy of Sciences of the United States of America 107, 3517–3521. [PubMed: 20133592]

[66]. Mohrmann R, de Wit H, Verhage M, Neher E and Sorensen JB (2010). Fast Vesicle Fusion in Living Cells Requires at Least Three SNARE Complexes. Science 330, 502–505. [PubMed: 20847232]

[67]. Sinha R, Ahmed S, Jahn R and Klingauf J (2011). Two synaptobrevin molecules are sufficient for vesicle fusion in central nervous system synapses. Proc Natl Acad Sci U S A 108, 14318–23. [PubMed: 21844343]

[68]. van den Bogaart G, Holt MG, Bunt G, Riedel D, Wouters FS and Jahn R (2010). One SNARE complex is sufficient for membrane fusion. Nature Structural & Molecular Biology 17, 358–U129.

[69]. Tong J, Borbat PP, Freed JH and Shin YK (2009). A scissors mechanism for stimulation of SNARE-mediated lipid mixing by cholesterol. Proc Natl Acad Sci U S A 106, 5141–6. [PubMed: 19251653]

[70]. Chapman ER (2008). How does synaptotagmin trigger neurotransmitter release? Annu Rev Biochem 77, 615–41. [PubMed: 18275379]

[71]. Perez-Lara A et al. (2016). PtdInsP2 and PtdSer cooperate to trap synaptotagmin-1 to the plasma membrane in the presence of calcium. Elife 5

[72]. (1986) Ion Channel Reconstitution, Plenum Press New York.

[73]. Gao Y, Zorman S, Gundersen G, Xi Z, Ma L, Sirinakis G, Rothman JE and Zhang Y (2012). Single reconstituted neuronal SNARE complexes zipper in three distinct stages. Science 337, 1340–3. [PubMed: 22903523]

[74]. Acuna C, Guo Q, Burre J, Sharma M, Sun J and Sudhof TC (2014). Microsecond dissection of neurotransmitter release: SNARE-complex assembly dictates speed and Ca(2)(+) sensitivity. Neuron 82, 1088–100. [PubMed: 24908488]

[75]. Zhao Y, Fang Q, Herbst AD, Berberian KN, Almers W and Lindau M (2013). Rapid structural change in synaptosomal-associated protein 25 (SNAP25) precedes the fusion of single vesicles with the plasma membrane in live chromaffin cells. Proc Natl Acad Sci U S A 110, 14249–54. [PubMed: 23940346]

[76]. Niles WD, Levis RA and Cohen FS (1988). Planar bilayer membranes made from phospholipid monolayers form by a thinning process. Biophys J 53, 327–35. [PubMed: 3349129]

[77]. Campillo C, Sens P, Koster D, Pontani LL, Levy D, Bassereau P, Nassoy P and Sykes C (2013). Unexpected membrane dynamics unveiled by membrane nanotube extrusion. Biophys J 104, 1248–56. [PubMed: 23528084]

[78]. Melikov KC, Frolov VA, Shcherbakov A, Samsonov AV, Chizmadzhev YA and Chernomordik LV (2001). Voltage-induced nonconductive pre-pores and metastable single pores in unmodified planar lipid bilayer. Biophys J 80, 1829–36. [PubMed: 11259296]

[79]. Ellens H, Bentz J, Mason D, Zhang F and White JM (1990). Fusion of influenza hemagglutinin-expressing fibroblasts with glycophorin-bearing liposomes: role of hemagglutinin surface density. Biochemistry 29, 9697–707. [PubMed: 2271610]

[80]. Melikyan GB, Niles WD and Cohen FS (1993). Influenza-Virus Hemagglutinin-Induced Cell-Planar Bilayer Fusion - Quantitative Dissection of Fusion Pore Kinetics into Stages. Journal of General Physiology 102, 1151–1170. [PubMed: 8133243]

[81]. Spruce AE, Iwata A and Almers W (1991). The first milliseconds of the pore formed by a fusogenic viral envelope protein during membrane fusion. Proc Natl Acad Sci U S A 88, 3623–7. [PubMed: 2023911]

[82]. Lindau M (2012). High resolution electrophysiological techniques for the study of calcium-activated exocytosis. Biochimica Et Biophysica Acta-General Subjects 1820, 1234–1242.

[83]. Curran MJ, Cohen FS, Chandler DE, Munson PJ and Zimmerberg J (1993). Exocytotic fusion pores exhibit semi-stable states. J Membr Biol 133, 61–75. [PubMed: 8320720]

[84]. Debus K and Lindau M (2000). Resolution of patch capacitance recordings and of fusion pore conductances in small vesicles. Biophys J 78, 2983–97. [PubMed: 10827977]

[85]. He LM, Wu XS, Mohan R and Wu LG (2006). Two modes of fusion pore opening revealed by cell-attached recordings at a synapse. Nature 444, 102–105. [PubMed: 17065984]

[86]. Ales E, Tabares L, Poyato JM, Valero V, Lindau M and de Toledo GA (1999). High calcium concentrations shift the mode of exocytosis to the kiss-and-run mechanism. Nature Cell Biology 1, 40–44. [PubMed: 10559862]

[87]. Dernick G, de Toledo GA and Lindau M (2003). Exocytosis of single chromaffin granules in cell-free inside-out membrane patches. Nature Cell Biology 5, 358–362. [PubMed: 12652310]

[88]. Chang CW, Hui E, Bai J, Bruns D, Chapman ER and Jackson MB (2015). A structural role for the synaptobrevin 2 transmembrane domain in dense-core vesicle fusion pores. J Neurosci 35, 5772–80. [PubMed: 25855187]

[89]. Tabares L, Lindau M and Alvarez de Toledo G (2003). Relationship between fusion pore opening and release during mast cell exocytosis studied with patch amperometry. Biochem Soc Trans 31, 837–41. [PubMed: 12887317]

[90]. Klyachko VA and Jackson MB (2002). Capacitance steps and fusion pores of small and large-dense-core vesicles in nerve terminals. Nature 418, 89–92. [PubMed: 12097912]

[91]. Albillos A, Dernick G, Horstmann H, Almers W, Alvarez de Toledo G and Lindau M (1997). The exocytotic event in chromaffin cells revealed by patch amperometry. Nature 389, 509–12. [PubMed: 9333242]

[92]. Hanna ST, Pigeau GM, Galvanovskis J, Clark A, Rorsman P and MacDonald PE (2009). Kiss-and-run exocytosis and fusion pores of secretory vesicles in human beta-cells. Pflugers Archiv-European Journal of Physiology 457, 1343–1350. [PubMed: 18795319]

[93]. Monck JR, Alvarez de Toledo G and Fernandez JM (1990). Tension in secretory granule membranes causes extensive membrane transfer through the exocytotic fusion pore. Proc Natl Acad Sci U S A 87, 7804–8. [PubMed: 2235997]

[94]. Solsona C, Innocenti B and Fernandez JM (1998). Regulation of exocytotic fusion by cell inflation. Biophys J 74, 1061–73. [PubMed: 9533718]

[95]. Wightman RM et al. (1991). Temporally Resolved Catecholamine Spikes Correspond to Single Vesicle Release from Individual Chromaffin Cells. Proceedings of the National Academy of Sciences of the United States of America 88, 10754–10758. [PubMed: 1961743]

[96]. Chow RH, von Ruden L and Neher E (1992). Delay in vesicle fusion revealed by electrochemical monitoring of single secretory events in adrenal chromaffin cells. Nature 356, 60–3. [PubMed: 1538782]

[97]. Zhou Z, Misler S and Chow RH (1996). Rapid fluctuations in transmitter release from single vesicles in bovine adrenal chromaffin cells. Biophysical Journal 70, 1543–1552. [PubMed: 8785312]

[98]. Dernick G, Gong LW, Tabares L, Alvarez de Toledo G and Lindau M (2005). Patch amperometry: high-resolution measurements of single-vesicle fusion and release. Nat Methods 2, 699–708. [PubMed: 16118641]

[99]. Wang CT, Lu JC, Bai JH, Chang PY, Martin TFJ, Chapman ER and Jackson MB (2003). Different domains of synaptotagmin control the choice between kiss-and-run and full fusion. Nature 424, 943–947. [PubMed: 12931189]

[100]. Alvarez de Toledo G, Fernandez-Chacon R and Fernandez JM (1993). Release of secretory products during transient vesicle fusion. Nature 363, 554–8. [PubMed: 8505984]

[101]. Wang CT, Grishanin R, Earles CA, Chang PY, Martin TF, Chapman ER and Jackson MB (2001). Synaptotagmin modulation of fusion pore kinetics in regulated exocytosis of dense-core vesicles. Science 294, 1111–5. [PubMed: 11691996]

[102]. Marszalek PE, Farrell B, Verdugo P and Fernandez JM (1997). Kinetics of release of serotonin from isolated secretory granules. II. Ion exchange determines the diffusivity of serotonin. Biophys J 73, 1169–83. [PubMed: 9284284]

[103]. Chow RH and von Ruden L (1995) Electrochemical detection of secretion from single cells In Single-Channel Recording (Sakmann B and Neher E, ed.^eds), pp. 245–275. Plenum Press, New York.

[104]. Schroeder TJ, Jankowski JA, Kawagoe KT, Wightman RM, Lefrou C and Amatore C (1992). Analysis of diffusional broadening of vesicular packets of catecholamines released from biological cells during exocytosis. Anal Chem 64, 3077–83. [PubMed: 1492662]

[105]. Nanavati C and Fernandez JM (1993). The secretory granule matrix: a fast-acting smart polymer. Science 259, 963–5. [PubMed: 8438154]

[106]. Marszalek PE, Farrell B, Verdugo P and Fernandez JM (1997). Kinetics of release of serotonin from isolated secretory granules. I. Amperometric detection of serotonin from electroporated granules. Biophys J 73, 1160–8. [PubMed: 9284283]

[107]. Gong LW, de Toledo GA and Lindau M (2007). Exocytotic catecholamine release is not associated with cation flux through channels in the vesicle membrane but Na(+) influx through the fusion pore. Nature Cell Biology 9, 915-+. [PubMed: 17643118]

[108]. Monck JR, Oberhauser AF, Alvarez de Toledo G and Fernandez JM (1991). Is swelling of the secretory granule matrix the force that dilates the exocytotic fusion pore? Biophys J 59, 39–47. [PubMed: 2015389]

[109]. Amatore C, Bouret Y, Travis ER and Wightman RM (2000). Interplay between membrane dynamics, diffusion and swelling pressure governs individual vesicular exocytotic events during release of adrenaline by chromaffin cells. Biochimie 82, 481–96. [PubMed: 10865134]

[110]. Mosharov EV and Sulzer D (2005). Analysis of exocytotic events recorded by amperometry. Nature Methods 2, 651–658. [PubMed: 16118635]

[111]. Glavinovic MI, Vitale ML and Trifaro JM (1998). Comparison of vesicular volume and quantal size in bovine chromaffin cells. Neuroscience 85, 957–68. [PubMed: 9639287]

[112]. Dunevall J, Fathali H, Najafinobar N, Lovric J, Wigstrom J, Cans AS and Ewing AG (2015). Characterizing the catecholamine content of single mammalian vesicles by collision-adsorption events at an electrode. J Am Chem Soc 137, 4344–6. [PubMed: 25811247]

[113]. Ren L et al. (2016). The evidence for open and closed exocytosis as the primary release mechanism. Q Rev Biophys 49, e12. [PubMed: 27659043]

[114]. Oleinick A, Svir I and Amatore C (2017). 'Full fusion' is not ineluctable during vesicular exocytosis of neurotransmitters by endocrine cells. Proceedings of the Royal Society a-Mathematical Physical and Engineering Sciences 473

[115]. Mellander LJ, Trouillon R, Svensson MI and Ewing AG (2012). Amperometric post spike feet reveal most exocytosis is via extended kiss-and-run fusion. Sci Rep 2, 907. [PubMed: 23205269]

[116]. Li X, Majdi S, Dunevall J, Fathali H and Ewing AG (2015). Quantitative measurement of transmitters in individual vesicles in the cytoplasm of single cells with nanotip electrodes. Angew Chem Int Ed Engl 54, 11978–82. [PubMed: 26266819]

[117]. Barg S, Olofsson CS, Schriever-Abeln J, Wendt A, Gebre-Medhin S, Renstrom E and Rorsman P (2002). Delay between fusion pore opening and peptide release from large dense-core vesicles in neuroendocrine cells. Neuron 33, 287–99. [PubMed: 11804575]

[118]. Karatekin E, Tran VS, Huet S, Fanget I, Cribier S and Henry JP (2008). A 20-nm step toward the cell membrane preceding exocytosis may correspond to docking of tethered granules. Biophysical Journal 94, 2891–2905. [PubMed: 18178647]

[119]. Tran VS, Huet S, Fanget I, Cribier S, Henry JP and Karatekin E (2007). Characterization of sequential exocytosis in a human neuroendocrine cell line using evanescent wave microscopy and "virtual trajectory" analysis. European Biophysics Journal with Biophysics Letters 37, 55–69. [PubMed: 17440716]

[120]. Taraska JW, Perrais D, Ohara-Imaizumi M, Nagamatsu S and Almers W (2003). Secretory granules are recaptured largely intact after stimulated exocytosis in cultured endocrine cells. Proc Natl Acad Sci U S A 100, 2070–5. [PubMed: 12538853]

[121]. Tsuboi T, McMahon HT and Rutter GA (2004). Mechanisms of dense core vesicle recapture following "kiss and run" ("cavicapture") exocytosis in insulin-secreting cells. J Biol Chem 279, 47115–24. [PubMed: 15331588]

[122]. Miesenbock G, De Angelis DA and Rothman JE (1998). Visualizing secretion and synaptic transmission with pH-sensitive green fluorescent proteins. Nature 394, 192–5. [PubMed: 9671304]

[123]. Anantharam A, Onoa B, Edwards RH, Holz RW and Axelrod D (2010). Localized topological changes of the plasma membrane upon exocytosis visualized by polarized TIRFM. J Cell Biol 188, 415–28. [PubMed: 20142424]

[124]. Llobet A, Wu M and Lagnado L (2008). The mouth of a dense-core vesicle opens and closes in a concerted action regulated by calcium and amphiphysin. J Cell Biol 182, 1017–28. [PubMed: 18779374]

[125]. Shin W and Gillis KD (2006). Measurement of changes in membrane surface morphology associated with exocytosis using scanning ion conductance microscopy. Biophys J 91, L63–5. [PubMed: 16844756]

[126]. Henkel AW and Almers W (1996). Fast steps in exocytosis and endocytosis studied by capacitance measurements in endocrine cells. Curr Opin Neurobiol 6, 350–7. [PubMed: 8794084]

[127]. Pickett JA and Edwardson JM (2006). Compound exocytosis: mechanisms and functional significance. Traffic 7, 109–16. [PubMed: 16420520]

[128]. Kasai H, Kishimoto T, Nemoto T, Hatakeyama H, Liu TT and Takahashi N (2006). Two-photon excitation imaging of exocytosis and endocytosis and determination of their spatial organization. Adv Drug Deliv Rev 58, 850–77. [PubMed: 16996640]

[129]. Zhang J and Castle D (2011). Regulation of fusion pore closure and compound exocytosis in neuroendocrine PC12 cells by SCAMP1. Traffic 12, 600–14. [PubMed: 21272170]

[130]. Bhat P and Thorn P (2009). Myosin 2 maintains an open exocytic fusion pore in secretory epithelial cells. Mol Biol Cell 20, 1795–803. [PubMed: 19158378]

[131]. Thorn P, Fogarty KE and Parker I (2004). Zymogen granule exocytosis is characterized by long fusion pore openings and preservation of vesicle lipid identity. Proc Natl Acad Sci U S A 101, 6774–9. [PubMed: 15090649]

[132]. Zhao WD et al. (2016). Hemi-fused structure mediates and controls fusion and fission in live cells. Nature 534, 548–52. [PubMed: 27309816]

[133]. Cardenas AM and Marengo FD (2016). How the stimulus defines the dynamics of vesicle pool recruitment, fusion mode, and vesicle recycling in neuroendocrine cells. J Neurochem 137, 867–79. [PubMed: 26849771]

[134]. Suchyna TM, Markin VS and Sachs F (2009). Biophysics and structure of the patch and the gigaseal. Biophys J 97, 738–47. [PubMed: 19651032]

[135]. Lollike K, Borregaard N and Lindau M (1998). Capacitance flickers and pseudoflickers of small granules, measured in the cell-attached configuration. Biophys J 75, 53–9. [PubMed: 9649367]

[136]. Hafez I, Kisler K, Berberian K, Dernick G, Valero V, Yong MG, Craighead HG and Lindau M (2005). Electrochemical imaging of fusion pore openings by electrochemical detector arrays. Proc Natl Acad Sci U S A 102, 13879–84. [PubMed: 16172395]

[137]. Meunier A et al. (2011). Coupling Amperometry and Total Internal Reflection Fluorescence Microscopy at ITO Surfaces for Monitoring Exocytosis of Single Vesicles. Angewandte Chemie-International Edition 50, 5081–5084. [PubMed: 21523868]

[138]. Sun XH and Gillis KD (2006). On-chip amperometric measurement of quantal catecholamine release using transparent indium tin oxide electrodes. Analytical Chemistry 78, 2521–2525. [PubMed: 16615759]

[139]. Kishimoto T, Kimura R, Liu TT, Nemoto T, Takahashi N and Kasai H (2006). Vacuolar sequential exocytosis of large dense-core vesicles in adrenal medulla. EMBO J 25, 673–82. [PubMed: 16467850]

[140]. Heuser JE and Reese TS (1973). Evidence for recycling of synaptic vesicle membrane during transmitter release at the frog neuromuscular junction. J Cell Biol 57, 315–44. [PubMed: 4348786]

[141]. Ceccarelli B, Hurlbut WP and Mauro A (1973). Turnover of transmitter and synaptic vesicles at the frog neuromuscular junction. J Cell Biol 57, 499–524. [PubMed: 4348791]

[142]. He L and Wu LG (2007). The debate on the kiss-and-run fusion at synapses. Trends Neurosci 30, 447–55. [PubMed: 17765328]

[143]. Rothman JE, Krishnakumar SS, Grushin K and Pincet F (2017). Hypothesis - buttressed rings assemble, clamp, and release SNAREpins for synaptic transmission. FEBS Lett 591, 3459–3480. [PubMed: 28983915]

[144]. Fang QH, Berberian K, Gong LW, Hafez I, Sorensen JB and Lindau M (2008). The role of the C terminus of the SNARE protein SNAP-25 in fusion pore opening and a model for fusion pore mechanics. Proceedings of the National Academy of Sciences of the United States of America 105, 15388–15392. [PubMed: 18829435]

[145]. Jorgacevski J et al. (2011). Munc18–1 Tuning of Vesicle Merger and Fusion Pore Properties. Journal of Neuroscience 31, 9055–9066. [PubMed: 21677188]

[146]. Kesavan J, Borisovska M and Bruns D (2007). v-SNARE actions during Ca(2+)-triggered exocytosis. Cell 131, 351–63. [PubMed: 17956735]

[147]. Dhara M et al. (2014). Complexin synchronizes primed vesicle exocytosis and regulates fusion pore dynamics. J Cell Biol 204, 1123–40. [PubMed: 24687280]

[148]. Bretou M, Anne C and Darchen F (2008). A fast mode of membrane fusion dependent on tight SNARE zippering. J Neurosci 28, 8470–6. [PubMed: 18716205]

[149]. Dhara M et al. (2016). v-SNARE transmembrane domains function as catalysts for vesicle fusion. Elife 5

[150]. Hastoy B et al. (2017). A Central Small Amino Acid in the VAMP2 Transmembrane Domain Regulates the Fusion Pore in Exocytosis. Sci Rep 7, 2835. [PubMed: 28588281]

[151]. Wang CT, Lu JC, Chapman ER, Martin TFJ and Jackson MB (2003). Synaptotagmin IV induces long-duration kiss-and-run exocytosis through small fusion pores. Biophysical Journal 84, 209a-209a.

[152]. Malsam J, Parisotto D, Bharat TAM, Scheutzow A, Krause JM, Briggs JAG and Sollner TH (2012). Complexin arrests a pool of docked vesicles for fast Ca2+-dependent release. Embo Journal 31, 3270–3281. [PubMed: 22705946]

[153]. Zhou Q, Zhou P, Wang AL, Wu D, Zhao M, Sudhof TC and Brunger AT (2017). The primed SNARE-complexin-synaptotagmin complex for neuronal exocytosis. Nature 548, 420–425. [PubMed: 28813412]

[154]. Kaeser PS and Regehr WG (2014). Molecular mechanisms for synchronous, asynchronous, and spontaneous neurotransmitter release. Annu Rev Physiol 76, 333–63. [PubMed: 24274737]

[155]. Ritchie TK, Grinkova YV, Bayburt TH, Denisov IG, Zolnerciks JK, Atkins WM and Sligar SG (2009). Reconstitution of Membrane Proteins in Phospholipid Bilayer Nanodiscs. Methods in Enzymol 464, 211–231. [PubMed: 19903557]

[156]. Shi L, Howan K, Shen QT, Wang YJ, Rothman JE and Pincet F (2013). Preparation and characterization of SNARE-containing nanodiscs and direct study of cargo release through fusion pores. Nat Protoc 8, 935–48. [PubMed: 23598444]

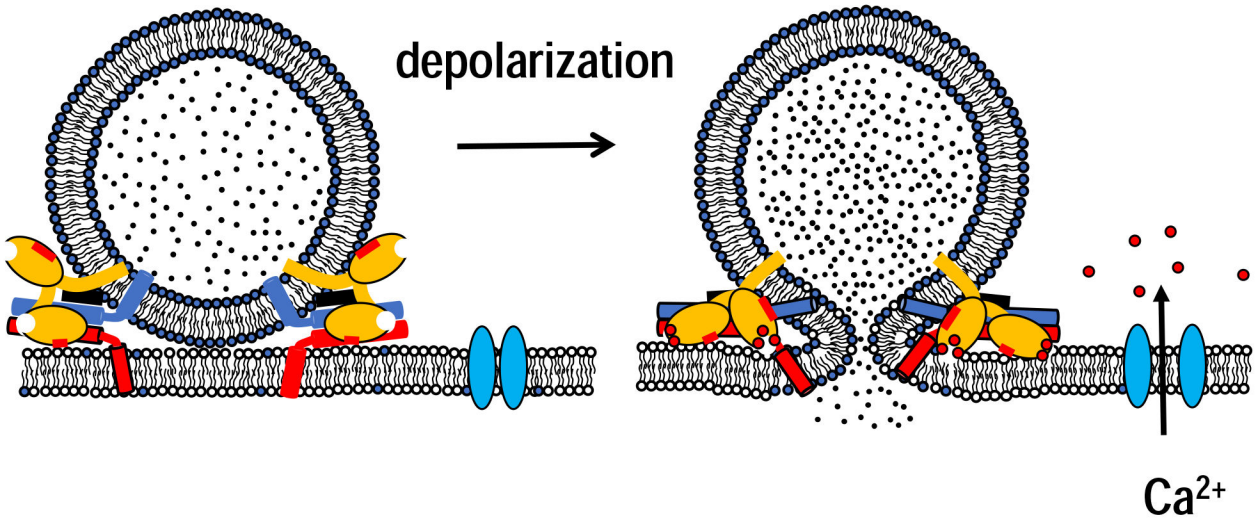

Figure 1.

Major players in calcium-triggered exocytosis. Formation of a complex between vesicular v- (red) and plasma membrane t-SNAREs (red) drives membrane fusion. Complex assembly is arrested at an intermediate stage by the synergistic action of Synaptotagmin (light orange) and complexin (black). Membrane depolarization opens voltage-gated calcium channels and allows rapid calcium influx. Tandem C2 domains of Synaptotagmin bind 2–3 calcium ions each and bury their hydrophobic residues at the tips of the calcium-binding loops into the bilayer. Other rearrangements likely allow further SNARE assembly and contribute to fusion pore opening.

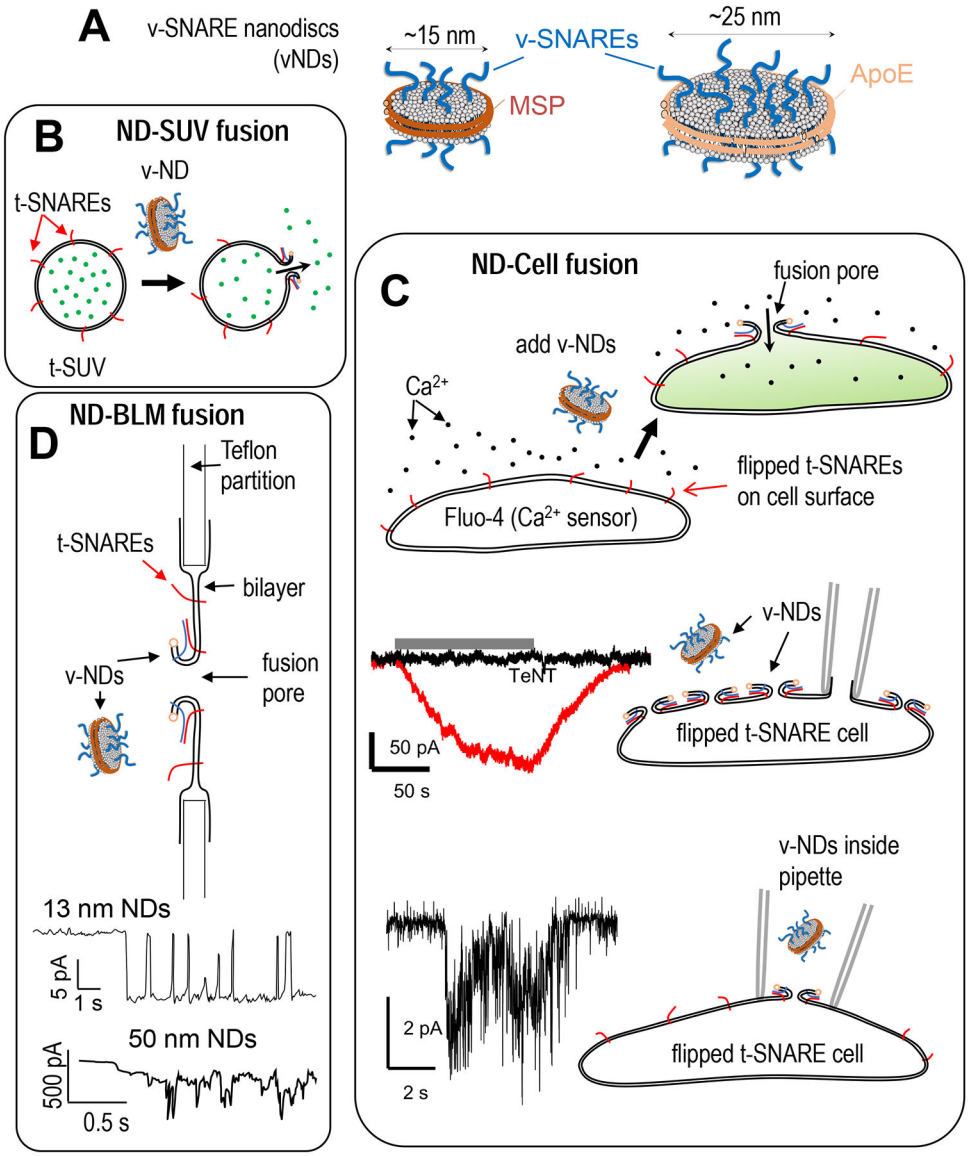

Figure 2.

Different types of nanodiscs reconstituted with the neuronal v-SNARE protein VAMP2/Synaptobrevin-2, and various nanodisc-based fusion assays. **A**. Left: MSP nanodiscs utilize an Apolipoprotein A1 derivative (membrane scaffold protein, MSP) to stabilize the edges of a flat phospholipid bilayer disc [47,155]. These discs are typically 13–17 nm in diameter and can accommodate 4–5 v-SNAREs per face [36,38,156]. Upon fusion of an MSP ND with a target membrane, the maximum size of the fusion pore that appears is limited to ~3–4 nm by the protein scaffold that forms a belt around the disc [36,38]. Right: Larger discs can be made using alternative scaffolds. ApoE-based scaffolds afford ~25 nm discs that can accommodate ~15 v-SNAREs per face [35,37]. With these discs, the fusion pore can expand to ≳ 10 nm diameter with little obstruction from the scaffold ring [35,37]. **B**. Nanodiscs reconstituted with neuronal v-SNAREs are mixed with small liposomes reconstituted with complementary neuronal t-SNAREs. Bulk cargo release is monitored by an increase in the

fluorescence of a cargo-sensitive dye present in the bath. Liposomes were loaded with calcium [36] or glutamate [40] and release was monitored using Mag-Fluo-4 or iGluSnFR, respectively. Release of sulforhodamine B from single t-SNARE liposomes upon fusion with v-SNARE NDs has also been monitored in a dye efflux assay using surface-tethered liposomes [41]. **C**. ND-cell fusion can be monitored in various manners [37,38,62]. Top: "flipped" t-SNARE cells [56] expressing complementary neuronal t-SNAREs ectopically with the SNARE domain facing the extracellular space, were fused with v-SNARE NDs [37,38]. The cells were pre-loaded with a calcium-sensitive fluorophore, Fluo-4. ND-cell fusion leads to calcium influx into the cytoplasm reported by an increase in Fluo-4 fluorescence. Middle: flipped t-SNARE cell under whole-cell voltage-clamp [38]. The patch pipette is depicted in gray. Perifusion of vNDs (grey bar) leads to a large whole-cell current (red trace) indicating opening of fusion pores on the cell surface. Application of vNDs treated with tetanus neurotoxin (TeNT) do not lead to currents (black trace). Figure modified from [38]. Bottom: single-pore conductance measurements using a flipped t-SNARE cell in the cell-attached patch configuration [37,38]. vNDs are included in the patch pipette. When a vND fuses with the cell surface, a fusion pore opens and allows direct-currents to be measured under voltage clamp. A representative trace is shown on the left (~16 nm diameter MSP vNDs, ~3–4 copies per ND face, transmembrane potential, −16 mV). **D**. Black-lipid membranes (BLMs) are single bilayer membranes that span a ~100–500 μm hole in a Teflon partition [72]. Recently they have been reconstituted with t-SNAREs and used as target membranes for fusion with ~13 nm v-SNARE NDs [41]. Current from a single fusion event is shown schematically. Currents in the ND-BLM assay have well-defined levels and flicker open-closed like ion channels, at least when pore size is confined by small NDs. When 50 nm diameter vNDs were used, fluctuating, larger currents with no evident stable levels were detected (bottom) [41].

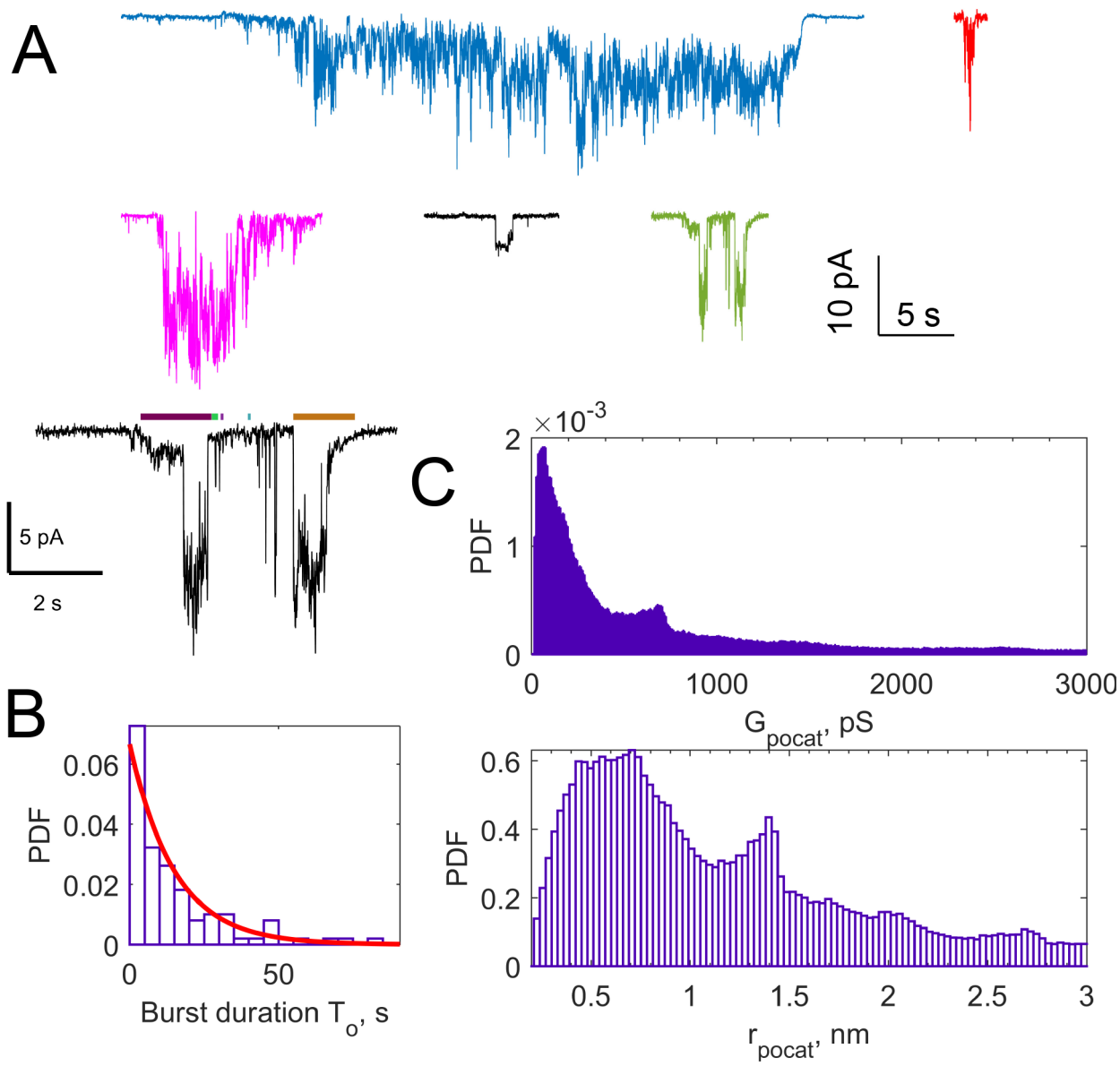

Figure 3.

Properties of single fusion pores. **A**. Examples of fusion pores that appear during ND-cell fusion, measured in cell-attached recordings. Large, ~25 nm NLPs loaded with ~15 copies per NLP face were used [37]. Most pores have fluctuating currents and no clear transitions between stable states. Some display preferred current levels, but such levels are not consistent across a given sample. The green example is replotted on a larger scale in black to show the threshold (red dashed lines) and a minimum threshold crossing time that are imposed to define open states (colored bars above traces). **B**. Lifetime distribution of ND-cell fusion pores, for NLPs loaded with 15 v-SNAREs per face. The exponential fit (red curve) resulted in a characteristic time of 15 s [37]. Pore lifetimes are ~6 s for smaller, MSP NDs loaded with 3–4 v-SNAREs per face [38]. **C**. Top: distribution of conductance values from 99 pores as in A. All points were concatenated to construct the distribution, so pores

lasting longer contributed more. Using a different averaging giving equal weight to every pore blunts the peak at ~700 pS. Bottom: distribution of pore sizes estimated from conductance data, assuming the pore is a 15 nm long cylinder [37,38].

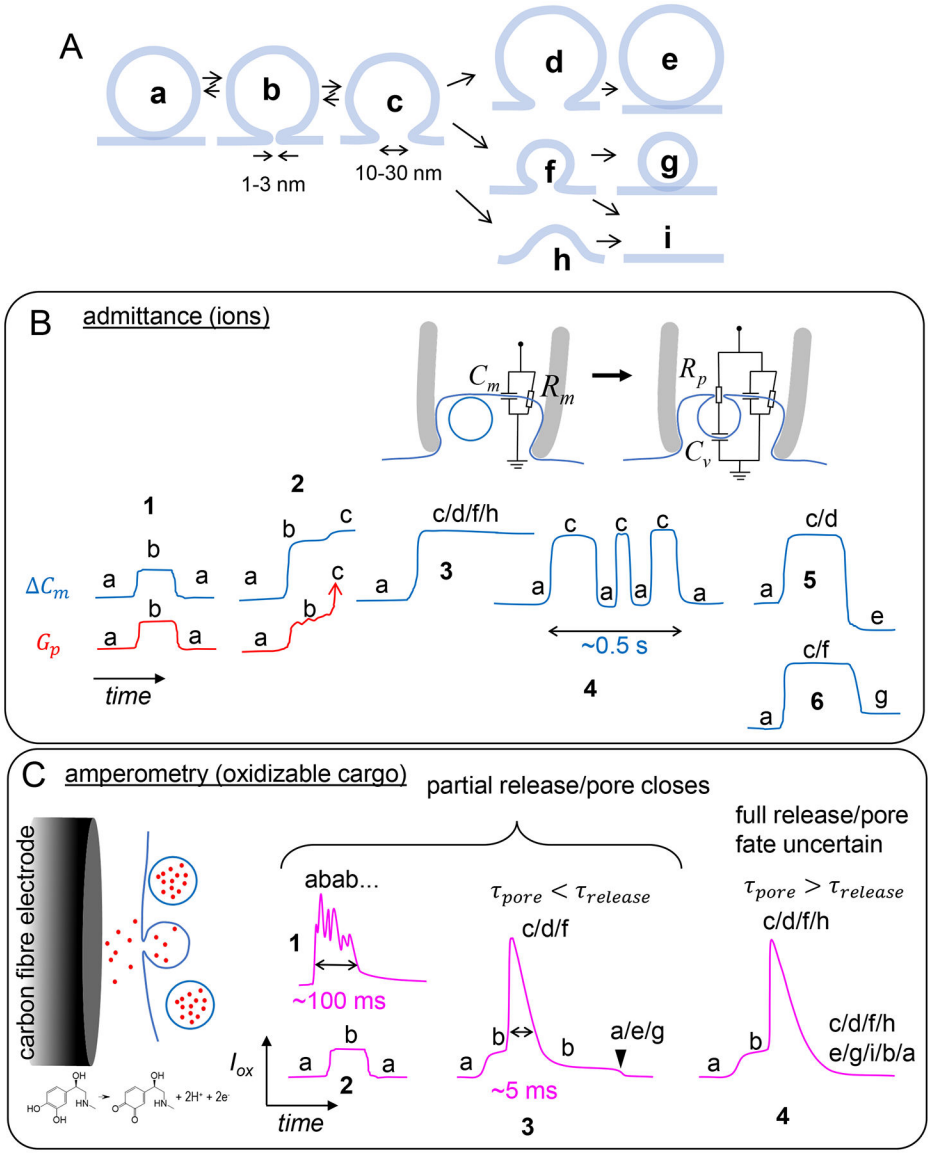

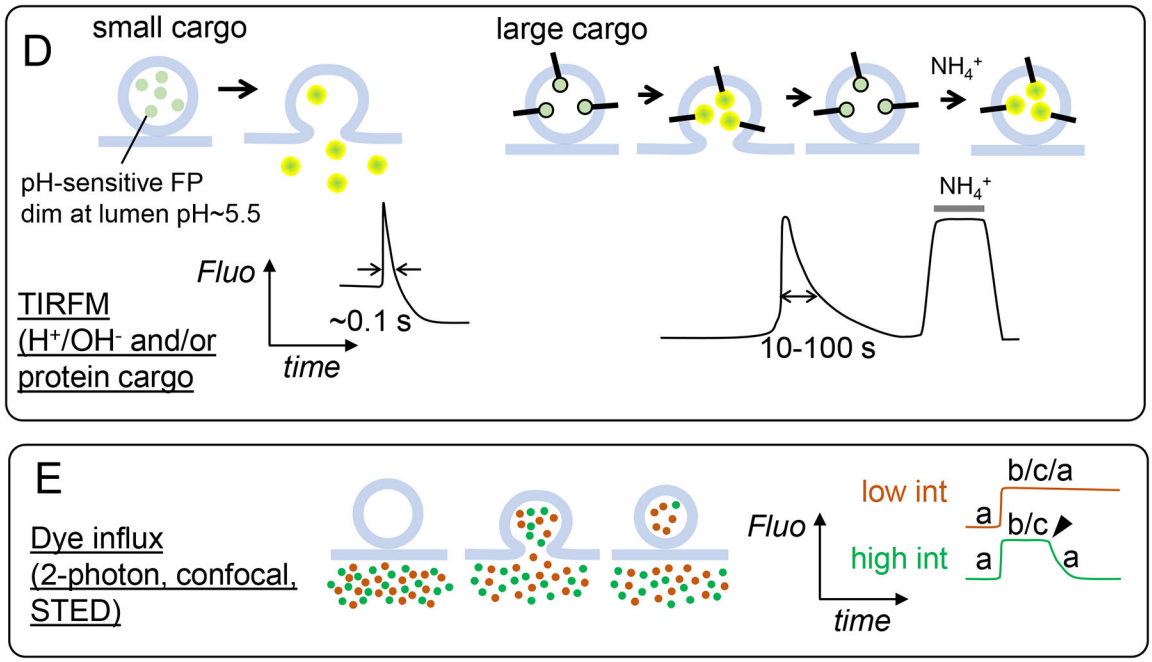

Figure 4.

Possible fates of the fusion pore and the fused vesicle, and how various methods would report them. **A**. Possible pathways that can be taken by the fusion pore and fused vesicle ghost. **B**. How the different pore/vesicle states in A (a-i) would appear in admittance measurements. ΔC_m and G_p refer to membrane capacitance (proportional to membrane area) and pore conductance (only detectable within a window, typically corresponding to pores $\lesssim$ 3 – 5 nm diameter), respectively. For small pores G_p may not be detected, depending on experimental parameters and vesicle size. Multiple states (e.g. “c/d/f/h”) indicate they would all produce the same signal, i.e. they could not be discriminated. Typical time resolution is 1–10 ms. **C**. Left: schematic of the detection principle. Released cargo such as catecholamines are oxidized as soon as they reach the surface of a carbon-fibre electrode, generating an oxidation current. Right: How the states depicted in A would appear in amperometric recordings of release, which have 0.1–1 ms time resolution. **D**. TIRFM detection of the states in A. Left: lumenal cargo is fused to a fluorescent protein (e.g. NPY-pHluorin). Upon fusion, the fluorescence of the granule rapidly increases (due to pH neutralization which enhances GFP fluorescence and release of the probe toward the glass surface where the evanescent field intensity is highest), then decreases due to diffusion of the labeled probes away from the fusion site. Right: if a slowly releasable cargo is fused to a pH sensitive fluorescent protein, signals increase due to pH neutralization after fusion, then return to baseline due to pore resealing and re-acidification. If the cargo is labeled with a pH-insensitive probe, or if the fluorescent probe is placed at the cytoplasmic end of a membrane cargo, then no signal is produced upon fusion up to >1 min [120]. Retention of cargo does not simply scale with cargo size; it can also be due to interactions with the dense-core matrix or membrane. To test how much, if any, of the cargo was lost during fusion, ammonium chloride is applied to collapse pH gradients. **E**. How dye influx measurements would report the states depicted in A. A mixture of dyes are placed in the extracellular bath.

Exocytosis allows both dyes to enter a granule, increasing the fluorescence intensity at the fusion site. One of the dyes (red) is excited at low power and probes the vesicle's size. The other (green) is excited at high power and probes when the fusion pore reseals. Pore resealing (arrowhead) prevents exchange of bleached dye with unbleached dyes in the bath and leads to a drop in the fluorescence intensity at the fusion site.